TECHNICAL REPORT R-92

AN INVESTIGATION OF THE EFFECT OF HIGH TEMPERATURE ON THE SCHUMANN-RUNGE ULTRAVIOLET ABSORPTION CONTINUUM OF OXYGEN

By JOHN S. EVANS and CHARLES J. SCHEXNAYDER, JR.

Langley Research Center
Langley Field, Va.

CONTENTS

TECHNICAL REPORT R–92

AN INVESTIGATION OF THE EFFECT OF HIGH TEMPERATURE ON THE SCHUMANN-RUNGE ULTRAVIOLET ABSORPTION CONTINUUM OF OXYGEN[1]

By JOHN S. EVANS and CHARLES J. SCHEXNAYDER, JR.

SUMMARY

A theoretical and experimental investigation has been carried out to determine the absorption coefficient of molecular oxygen at high temperature. The wavelength range was chosen to cover the Schumann-Runge continuum between 1,300 and 1,750 angstrom units. The theoretical investigation covered temperatures from 300° to 10,000° K. The experimental investigation was carried out in the range from 4,000° to 10,000° K. All values of the absorption coefficient found apply only to oxygen for which the vibrational degree of freedom is fully excited.

Three types of theoretical calculations were carried out: (1) "reflection" of the ground-state wave functions by the potential curve for the excited state, (2) calculation on an IBM 704 electronic data processing machine of vibrational overlap integrals with Morse eigenfunctions being used for the ground-state wave functions and computed solutions of the Schrödinger equation being used for the excited-state wave functions, and (3) use of a simplified formula for the absorption coefficient which is applicable (at least in principle) to all diatomic molecules at all temperatures. An empirical correction for the variation of electronic transition probability with internuclear distance was also included and was found to improve the agreement between theory and experiment.

The experimental investigation was carried out by using a 1-inch-diameter shock tube to produce high-temperature samples of oxygen, air, and a mixture of 10-percent oxygen in argon. The absorption in a 1- by 3-millimeter beam of ultraviolet light was recorded as a function of time during the passage of shock waves.

The experimental measurements exhibited considerable scatter, which was attributed chiefly to unsteadiness of the light source. Nevertheless, the general agreement of measurements with calculations was adequate to show that the method of calculation is valid and that the magnitude and temperature dependence of the theoretically determined coefficient are essentially correct for wavelengths larger than 1,375 angstrom units. Below this wavelength the absorption coefficient values given are estimates based on a few experimental points.

The measured absorption coefficient generally was larger in oxygen-argon mixtures than that predicted by theory, whereas it was smaller in pure oxygen. The discrepancy between theory and experiment could not be accounted for in the pure-oxygen results, but it was largely removed for the oxygen-argon results when the theoretical coefficients were recalculated on the assumption that only the ground electronic state of the oxygen molecule was excited immediately behind the shock front. Best agreement between theory and experiment for the pure oxygen results was obtained by retaining the original assumption of complete electronic excitation of oxygen immediately behind the shock front.

No absorption coefficients were obtained from the tests made in air because the adjustment of nitrogen vibration interfered with the accurate determination of the jump in light intensity across the shock front. The air data are reported and discussed, however, because of the light they throw on the measurements in oxygen and in oxygen-argon mixtures.

[1] The information in this paper is largely based on a dissertation submitted by John S. Evans in partial fulfillment of the requirements for the degree of Doctor of Philosophy in Physics, University of Tennessee, Knoxville, Tennessee, December 1959.

INTRODUCTION

The absorption coefficient of a gas for light of a given wavelength is commonly defined by the relation

$$J = J_o e^{-k\hat{\rho}l} \tag{1}$$

where J and J_o are the transmitted and incident intensities of the light, respectively, k is the absorption coefficient per centimeter, and $\hat{\rho}l$ is the thickness in centimeters of the absorbing gas layer reduced to standard density. The absorption coefficient for a given gas is a function of the gas temperature and of the wavelength of the light. Figure 1 is intended to illustrate the general effect of these parameters on an absorption continuum like that found in oxygen. The wavelength dependence is such that the absorption coefficient has a maximum value at a particular wavelength and falls off to either side. Increasing the temperature has three effects:

(1) The magnitude of the peak decreases
(2) The position of the peak shifts to shorter wavelengths
(3) The range over which absorption occurs spreads out to both longer and shorter wavelengths

The oxygen continuum with which this report is concerned has a peak between 1,400 and 1,500 angstrom units and at room temperature extends from 1,300 to 1,750 angstrom units. One of the reasons for attempting a quantitative evaluation of the effect of high temperature on this absorption continuum is that the absorption can be used to follow rapid changes in the concentration of molecular oxygen, such as those which occur in fast chemical reactions behind shock waves. Since the oxygen involved in these processes is at a much higher temperature than that at which presently existing measurements of the absorption coefficient were made, knowledge of the temperature dependence of the absorption coefficient is needed.

Values of the absorption coefficient measured at room temperature are listed in references 1 to 6. These data are shown in figure 2. The two curves which also appear in figure 2 are the results of two theoretical calculations (refs. 7 and 8). Stueckelberg's curve was calculated specifically for oxygen, but the other curve is an application to oxygen of a general formula derived by Sulzer and Wieland for calculating the absorption coefficient of a diatomic gas at any temperature from a knowledge of its absorption at 0° K and its characteristic vibrational temperature. Camac and Vaughan (ref. 9) have published experimentally determined values at 1,470 angstrom units for temperatures up to 8,000° K. Their measurements largely substantiate both the theoretical and experimental results given herein. The slight differences noted

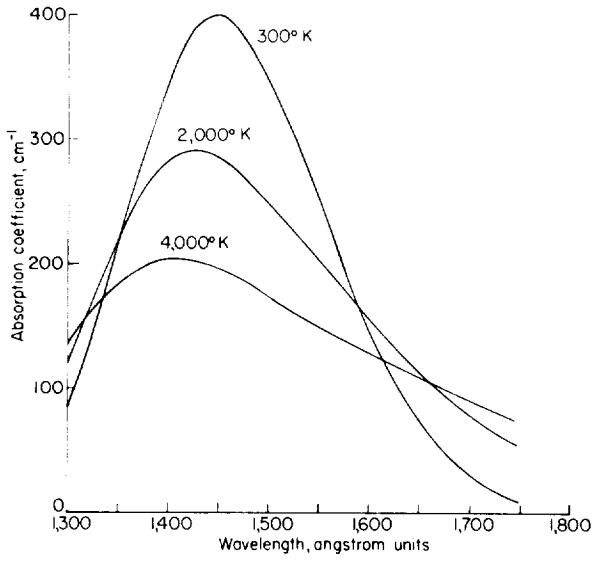

FIGURE 1.—Absorption coefficient of molecular oxygen. Typical curves.

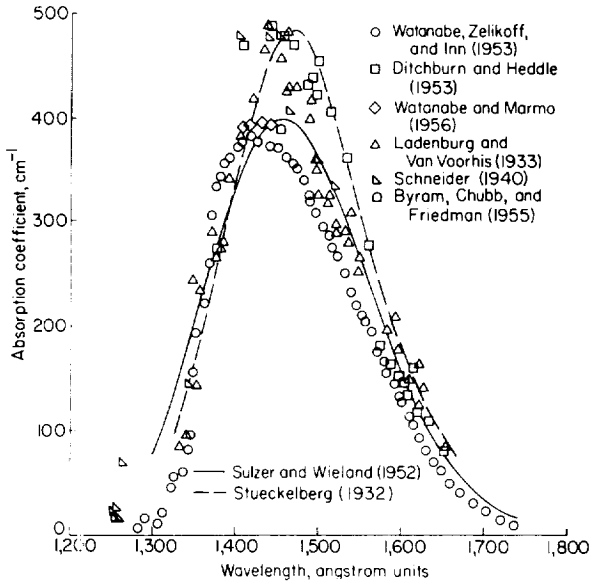

FIGURE 2.—Absorption coefficient of molecular oxygen; measured values at room temperature.

are discussed in the section entitled "Discussion of Results."

The only other results given in the literature with which the work reported here could be compared were those obtained by using the formula of Sulzer and Wieland. In references 10 to 16 absorption coefficients calculated from this formula agreed well with measured values for chlorine, iodine, and bromine at temperatures up to 2,000° K. Some typical curves and experimental data from these papers are shown in figures 3 and 4.

In this report both experimental and theoretical approaches are made to the problem of determining the absorption coefficient of oxygen at high temperature. High-temperature oxygen was obtained by means of the compression occurring in a shock wave passing through oxygen contained in a steel tube. The gas was heated to temperatures in the range of 4,000° to 10,000° K in a time which was short compared with the instrumental resolving time of the order of a few tenths of a microsecond. Light intensity as a function of time was displayed on an oscilloscope screen and photographed.

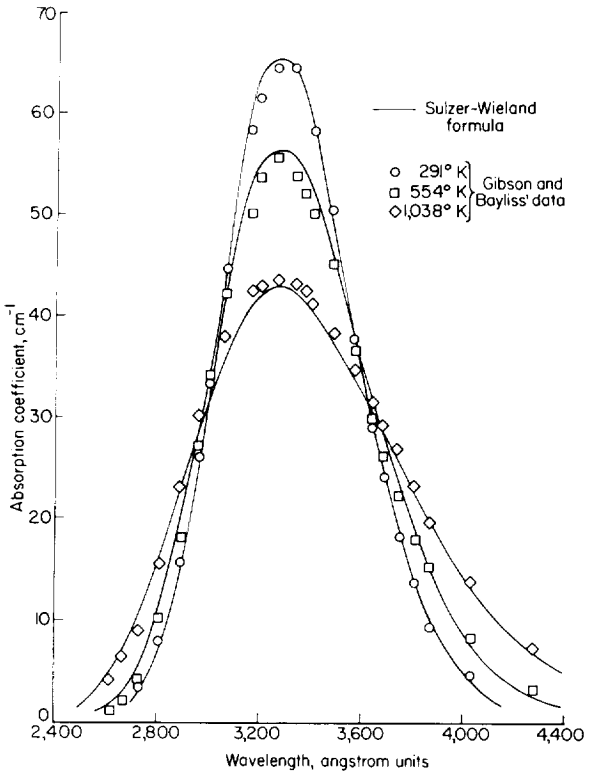

FIGURE 3.—Absorption coefficient of molecular chlorine.

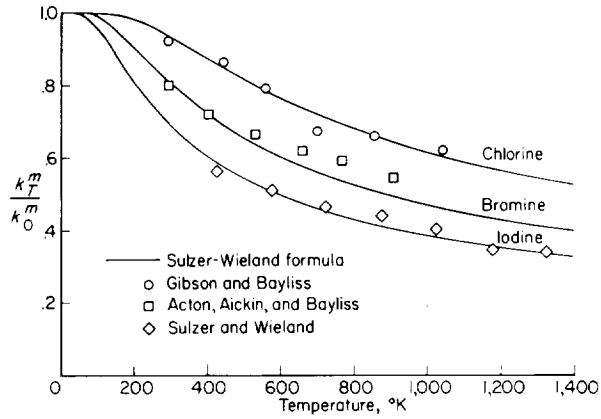

FIGURE 4.—Temperature dependence of absorption-curve peaks.

In the theoretical approach three calculations were made. They were:

(1) The reflection or delta function method
(2) A more elaborate calculation in which a digital computer was used
(3) Substitution into the formula of Sulzer and Wieland

SYMBOLS

$A_{v''}$ normalization factor for the Morse eigenfunctions, $[\beta(x_e^{-1}-2v''-1)(v'')!/\Gamma(x_e^{-1}-v'')]^{1/2}$

a speed of sound, cm/sec

$\tilde{a}$ slope of potential curve for $B(^3\Sigma_u^-)$ state at r_s, erg per angstrom unit

B_e spectroscopic constant, rotational frequency, $h/8\pi^2cI_e$, cm^{-1}

C_1, C_2, C_3, C_4 experimentally determined proportionality constants (eqs. (8) and (11) and appendix A)

c velocity of light, 2.9979×10^{10} cm/sec

D_e dissociation energy of the oxygen molecule in the $X(^3\Sigma_g^-)$ state measured from the minimum of the potential curve, 42,048 cm^{-1}

d diameter of Rowland circle, equals radius of curvature of diffraction grating, 39.888 cm (fig. 26)

E vibrational kinetic energy, erg

E^* energy of absorbed light quantum, $h\nu$, erg

$\tilde{E}$ energy of final state measured from dissociation level of $B(^3\Sigma_u^-)$ state, erg

F normalization factor for ψ wave function, $241.89\tilde{E}^{1/4}\tilde{a}^{-1/6}$

G energy of vibrational levels referred to $v''=0$ level as zero level, cm^{-1}

g mole fraction of oxygen in initial gas mixture (for oxygen, $g=1.00$; for air, $g=0.21$; for oxygen-argon, $g=0.1007$)

h Planck's constant, 6.6253×10^{-27} erg-sec

I_e moment of inertia of the molecule, μr_e^2, gram-cm^2

i angle of incidence (fig. 26)

J intensity of transmitted light, erg/cm^2-sec

J_o intensity of incident light, erg/cm^2-sec

K rotational quantum number

k absorption coefficient, cm^{-1}

$k_{v''}(\lambda)$ absorption coefficient of molecules in v'' level as a function of λ, cm^{-1}

$k_T(\lambda)$ absorption coefficient of oxygen as a function of wavelength at temperature T, cm^{-1}; $k_T(\lambda)=\sum N_{v''}(T)k_{v''}(\lambda)$

$k_T(\tilde{\nu})$ absorption coefficient of oxygen as a function of wave number at temperature T, cm^{-1}

$\hat{k}_{v''}(\lambda)=k_{v''}(\lambda)/k_0^m$

$\hat{k}_T(\lambda)=k_T(\lambda)/k_0^m$

$\hat{k}_T(\tilde{\nu})=k_T(\tilde{\nu})/k_0^m$

k_0^m maximum value of $k_T(\lambda)$ curve at 0° K, equals (essentially) peak value of k at room temperature, 400 cm^{-1}

l absorption path length, cm

M_{I} shock Mach number, $u_{\mathrm{I}}/a_{\mathrm{I}}$

M_{II} dimensionless velocity of flow behind shock, $u_{\mathrm{II}}/a_{\mathrm{I}}$

$N_{v''}(T)$ weighting factor for $k_{v''}(\lambda)$, represents equilibrium population of ground-state vibrational levels, $(1/S)\exp(G_{v''}hc/\kappa T)$

n diffraction order (fig. 26)

p pressure, dyne/cm^2

$Q_{v''}$ associated Laguerre polynomial,

$$Q_{v''}=\frac{\Gamma(x_e^{-1}-v'')\sum_{j=0}^{v''}\{(-1)^j x_e^{-j}\exp[-j\beta(r-r_e)]\}}{[j!(v''-j)!\Gamma(x_e^{-1}-2v''+j)]}$$

R gas constant per unit mass

r distance between oxygen atoms in oxygen molecule, angstrom units or cm

S partition function for vibrational levels of three lowest electronic states of oxygen,

$$S=\sum\exp(-G_{v''}hc/\kappa T)+\frac{2}{3}\sum\exp(-G_{va}hc/\kappa T)+\frac{1}{3}\sum\exp(-G_{vb}hc/\kappa T)$$

s distance between lines on diffraction grating, 1.693×10^{-4} cm (fig. 26)

T temperature, °K

u gas flow velocity, cm/sec

V vibrational potential energy, erg

v vibrational quantum number

$x_e=\omega_e x_e/\omega_e=0.0076345$

x_1, x_2 distances locating entrance and exit slits, respectively (fig. 26)

y distance of entrance and exit slits from monochromator center line (fig. 26)

α degree of dissociation

β Morse function constant for $X(^3\Sigma_g^-)$ state, per angstrom unit ($\beta=4(0.12177)(2\omega_e x_e)^{1/2}=2.3935$ was used in the calculations; however, $\beta=0.12177\omega_e(\mu/D_e)^{1/2}=2.6544$ is better for plotting the whole Morse curve)

γ ratio of specific heat at constant pressure to specific heat at constant volume

ϵ angle between grating normal and monochromator centerline (fig. 26)

ζ diffraction angle (fig. 26)

η dimensionless enthalpy, $\dfrac{\text{Enthalpy}}{RT}$

Θ characteristic vibrational temperature for $X(^3\Sigma_g^-)$ state, 2,260° K

κ Boltzmann's constant, 1.3804×10^{-16} erg/deg

λ wavelength of light, angstrom units

μ reduced mass of oxygen atom, 1.328×10^{-23} gm

ν frequency of absorbed light quantum, sec^{-1}

$\tilde{\nu}$ wave number, $1/\lambda$, cm^{-1}

$\tilde{\nu}_m$ wave number corresponding to maximum of $k_T(\tilde{\nu})$ curve at 0° K, 69,000 cm^{-1}

$\Delta\tilde{\nu}_0$ natural half breadth of $k_T(\tilde{\nu})$ curve at 0° K, 6,481 cm^{-1}

ρ gas density, $gram/cm^3$

$\hat{\rho}$ reduced gas density, $g\rho/\rho_s$

σ density ratio across shock front, ρ_{II}/ρ_I

ϕ normalized Morse vibrational wave function for $X(^3\Sigma_g^-)$ state

ψ unnormalized vibrational wave function for $B(^3\Sigma_u^-)$ state

Ω electronic transition probability for $X(^3\Sigma_g^-) \leftarrow B(^3\Sigma_u^-)$

ω_e spectroscopic constant of $X(^3\Sigma_g^-)$ state, vibrational frequency, 1,580.361 cm^{-1}

$\omega_e x_e$ spectroscopic constant of $X(^3\Sigma_g^-)$ state, anharmonicity correction, 12.0730 cm^{-1}

Subscripts:

I gas immediately in front of shock

II gas immediately behind shock

e minimum of vibrational potential curve

max maximum

s gas at 273.2° K and 1 atmosphere pressure or turning point of vibrational motion in the $B(^3\Sigma_u^-)$ state, as appropriate

v vibrational quantum number

Superscripts:

$'$ upper state of Schumann-Runge transition, that is, the $B(^3\Sigma_u^-)$ state

$''$ lower state of Schumann-Runge transition, that is, the $X(^3\Sigma_g^-)$ state

a the $a(^1\Delta_g)$ electronic state of O_2

b the $b(^1\Sigma_g^+)$ electronic state of O_2

THEORETICAL CALCULATION OF ABSORPTION COEFFICIENT

BACKGROUND MATERIAL

Discussion of molecular state transitions responsible for Schumann-Runge absorption.—The absorption continuum under study adjoins the Schumann-Runge molecular band system in oxygen (discussed in ref. 17, p. 446) and is due to the same electronic transition. Each electronic state of a diatomic molecule has a characteristic potential energy associated with the vibration of the nuclei along the line joining their centers. The vibrational potential energy curves for the five known electronic states of the O_2 molecule are shown in figure 5. Morse functions (discussed in ref. 17, p. 101) were used; the constants were obtained from reference 17 (p. 560) except for the dissociation energy D_e which was obtained from reference 18.

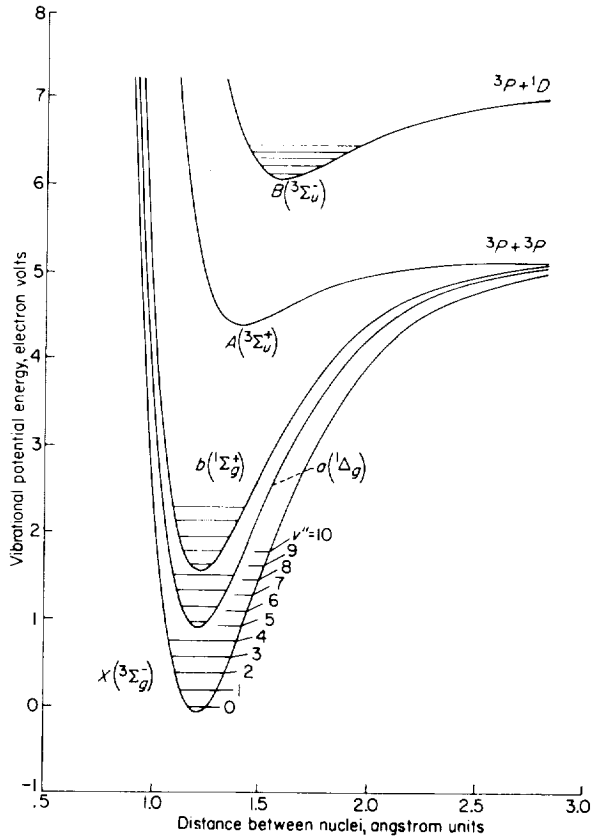

FIGURE 5.—Vibrational potential energy of the oxygen molecule.

The three kinds of molecular energy which are involved in the transitions responsible for the Schumann-Runge band system are the electronic, vibrational, and rotational energy changes. A short discussion of each of these follows.

Electronic energy changes are represented by vertical distances between the potential curves of figure 5. The only transition between the known electronic states of oxygen which is allowed by strict application of the selection rules (ref. 17, p. 240) is the $B(^3\Sigma_u^-) \leftarrow X(^3\Sigma_g^-)$ transition which gives rise to the Schumann-Runge band system. Since the selection rules are not completely obeyed, other transitions between these states do occur, but the absorption and emission due to them are weak.

Some of the vibrational energy levels of the states are also shown in figure 5. The individual absorption bands of the Schumann-Runge system

are due to transitions which originate in one of the vibrational levels of the $X(^3\Sigma_g^-)$ state and terminate in one of the vibrational levels of the $B(^3\Sigma_u^-)$ state. The absorption continuum is due to the same transitions except that the final state lies above the dissociation limit of the B state. Molecules which have absorbed light in the continuum immediately dissociate into one normal ^3P and one excited ^1D atom (ref. 17, p. 447). In electronic transitions there is no strict selection rule for the vibrational quantum number (ref. 17, p. 194).

Examination of the individual bands in a molecular band system with a spectroscope of high resolving power reveals a fine structure which is attributed to rotation of the molecules. Figure 6 shows some of the rotational levels associated with the $v''=0$ and $v''=10$ vibrational levels of the X state of O_2. The selection rules for rotational transitions (ref. 17, p. 244) limit changes in the rotational quantum number between Σ states to $\Delta K=\pm 1$. This limitation, plus the fact that the rotational energy level spacing is small compared with the spacing of electronic and vibrational levels, made it possible to neglect the effect of the change in rotational energy on the calculation of the absorption coefficient in the continuum.

Distribution of molecules over vibrational states. At 0° K all the O_2 molecules in a given sample are in the $v''=0$ level of the X state. In order to calculate the absorption coefficient at 0° K only transitions originating in this lowest state need to be considered. At higher temperatures transitions from excited vibrational states have to be taken into account. To do this the absorption coefficient was calculated for each initial state as if it were the only one and the overall absorption coefficient was found by adding the contributions from all the states. Numbers representing the population of the initial levels under the assumption of vibrational equilibrium were used as weighting factors. The expression used for calculating the weighting factors was

$$N_{v''}(T)=(1/S)\exp(-G_{v''}hc/\kappa T) \qquad (2)$$

where

$$S=\sum \exp(-G_{v''}hc/\kappa T)+\frac{2}{3}\sum \exp(-G_{v^a}hc/\kappa T)+\frac{1}{3}\sum \exp(-G_{v^b}hc/\kappa T)$$

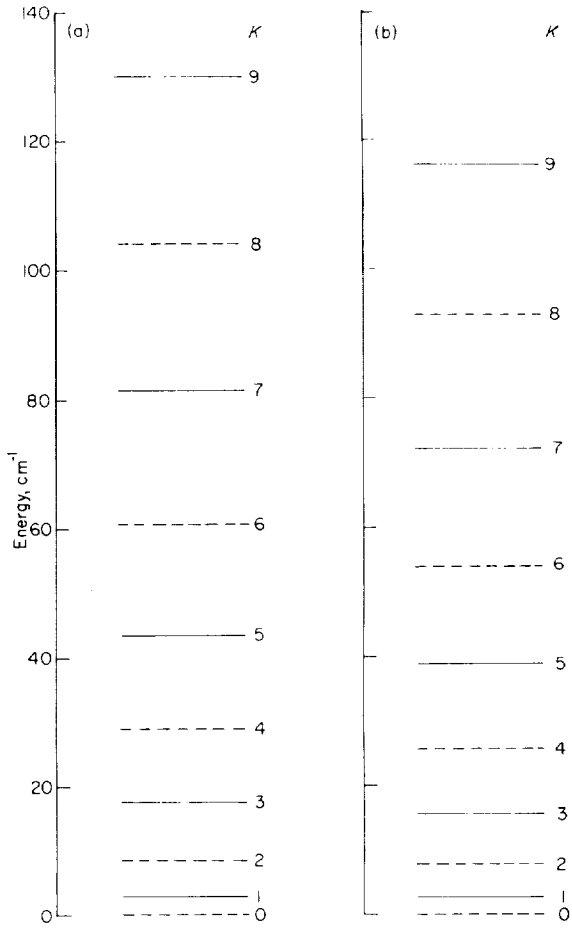

(a) $v''=0$. (b) $v''=10$.

FIGURE 6.—Rotational energy levels of $v''=0$ and $v''=10$ vibrational levels of X state of oxygen. Dashed lines indicate that transitions involving these levels do not appear in the spectrum. (Term value $=B_{v''}K(K+1)$, where $B_0=1.438$ cm^{-1} and $B_{10}=1.280$ cm^{-1}.)

$G_{v''}$=energy of v'' level (referred to $v''=0$ as the zero level), cm^{-1}; $G_{v^{a,b}}$=energy of $v^{a,b}$ level (referred to $v''=0$ as the zero level), cm^{-1}.

Note that vibrational levels of the $a(^1\Delta_g)$ and $b(^1\Sigma_g^+)$ states were included in the partition function S. Absorption of light by these states is negligible and it is not necessary to consider them in calculating the overall coefficient except for their appearance in the partition function.

Evidence will be cited for believing that, while the a and b states are excited immediately behind a shock wave in oxygen, they are not excited behind a shock wave in oxygen-argon mixtures. Figure 7 shows the $S(T)$ values appropriate to each of these assumptions.

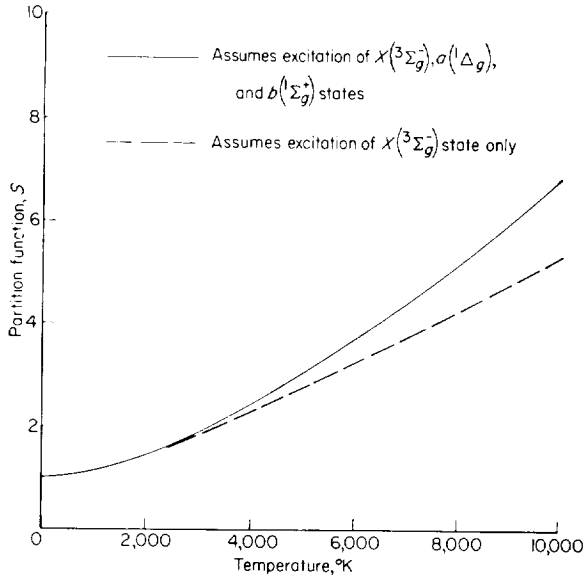

FIGURE 7.—Vibrational partition function for oxygen.

The equilibrium population of the vibrational levels of the X, a, and b states is shown in figure 8 for 5,000° and 10,000° K. The population of the rotational states of the $v''=0$ and $v''=10$ levels of the X state is shown for the same temperatures in figure 9.

The Franck-Condon principle.—The absence of selection rules for vibrational quantum number changes occurring in electronic transitions has already been mentioned. The observed intensity distributions are adequately explained by the

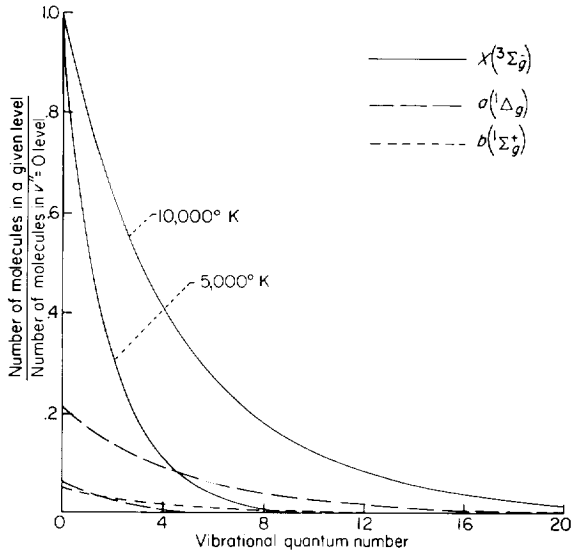

FIGURE 8.—Relative population of vibrational levels.

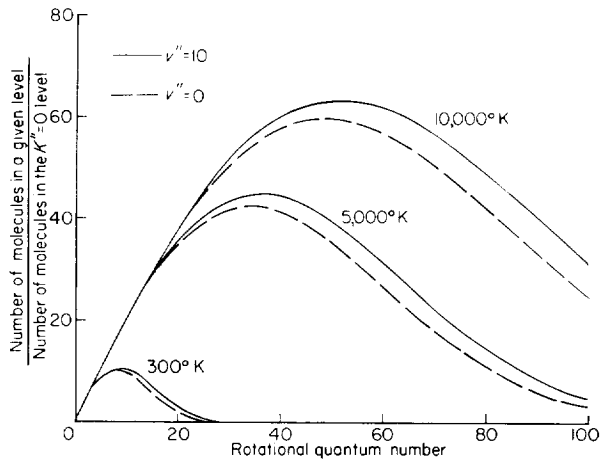

FIGURE 9.—Relative population of rotational levels.

quantum mechanical formulation of the Franck-Condon principle (discussed in ref. 17, p. 199, and in ref. 19). The main idea in this principle is that the electrons move so rapidly compared with the heavy nuclei that the positions and velocities of the nuclei are unchanged in an electronic transition. From the viewpoint of classical mechanics the nuclei spend most of their time near the turning points of the vibrational motion, where they have zero velocity. Thus, the most probable transitions are those for which a turning point of the upper state occurs at the same internuclear distance as a turning point of the lower state. In the quantum mechanical formulation the transition probability is proportional to the square of the vibrational overlap integral $\int_0^\infty \phi(r)\psi(r)dr$, where $\phi(r)$ is the vibrational wave function for the lower state and $\psi(r)$ is the vibrational wave function for the upper state. If $\phi(r)$ and $\psi(r)$ are replaced by delta functions located at the turning points, the classical Franck-Condon result is obtained.

The following expression for the absorption coefficient is based on equations given in reference 17 (pp. 201 and 383):

$$k_{v''}(\lambda) = (\text{Constant})(\Omega E^* \tilde{E}^{-1/2}) \left(F \int_0^\infty \phi_{v''} \psi dr \right)^2 \quad (3)$$

The factor E^* is the energy of the absorbed light quantum. The factor F is a normalization factor for the upper-state wave function ψ and is defined subsequently. The factor $\tilde{E}$ is the energy of the oxygen molecule in the final state measured from the asymptote of the $B(^3\Sigma_u^-)$ curve. This factor

is not present in the expression for the absorption coefficient for a discrete band but does appear in the corresponding expression for a continuum. This is pointed out on pages 196 and 202 of reference 19, but is not mentioned in the discussion of continuum absorption given on page 391 of reference 17. The latter treatment is not in error, however, because the $\tilde{E}$ factor cancels out when the normalization of the ψ function is considered.

The factor Ω is the transition probability for the electronic transition $X(^3\Sigma_g^-) \leftarrow B(^3\Sigma_u^-)$ and is customarily assumed to be a constant. Theoretical calculation of its variation with internuclear distance is impractical because the necessary electronic wave functions are not known, but some empirical treatments have been given (ref. 19, p. 208; refs. 20 and 21). Herzberg (ref. 17, p. 394) points to the excellent quantitative agreement often obtained between theory and experiment as justification for neglecting this factor. Since there is no reason why Ω should be a function of temperature, good agreement obtained between theory and experiment at room temperature can be used as a criterion of the adequacy of the assumption that it is constant. Conversely, by assuming that any discrepancies present at room temperature are due to this assumption, the variation of Ω with internuclear distance can be calculated. The approach used here is to follow the usual procedure of assuming that Ω is constant and then later to introduce an empirical correction factor based on a comparison of theory and experiment at room temperature.

Discussion of effect of neglecting rotation of molecules.—Equation (3) ignores the rotation of the molecules. This is commonly done in order to cut down on the labor of the computations and, for molecules with deep potential wells, does not lead to large errors. The following discussion of the considerations involved is similar to one given in reference 10.

For a rotating vibrator centrifugal forces are acting on the nuclei in addition to the usual restoring forces. The result is that the vibrational motion takes place under the influence of an effective potential given by the equation (ref. 17, p. 426)

$$V_K(r) = V_0(r) + (B_e r_e^2/r^2)K(K+1) \qquad (4)$$

where $V_0(r)$ is the potential curve for the rotationless state, B_e is the rotational constant $h/8\pi^2 c I_e$, K is the rotational quantum number, and I_e is the moment of inertia of the molecule. Figure 10 shows some of these curves for the X and B states of oxygen.

Most of the rotating molecules in the 11 lowest vibrational levels of the X state have rotational quantum numbers of the order of $K=50$ at a temperature of 10,000° K. For the X state the minimum of the effective potential curve as compared with that of the rotationless state is shifted up by 3,574 cm^{-1} and to the right from 1.207 to 1.220 angstrom units. At the left extremity of r values used ($r=1.08$ angstrom units) the curve is shifted up by 4,514 cm^{-1} and at the right extremity ($r=1.32$ angstrom units) it is shifted up by 3,022 cm^{-1}. The net effect on the shape of the curve when the upward shift of the minimum is subtracted out is an upward shift of 940 cm^{-1} at the left extremity and a downward shift of 572 cm^{-1} at the right extremity plus a shift to the right of the minimum of 0.013 angstrom unit. The vertical changes amount to about 2 percent of the depth of the potential well and the horizontal shift of the minimum to about 5 percent of the range of r values used. The effect on the B state is almost exactly the same. The left extremity is raised by 4,516 cm^{-1} (compared with 4,514 cm^{-1} for the X state) and the right extremity is raised by 3,024 cm^{-1} (compared with 3,022 cm^{-1} for the

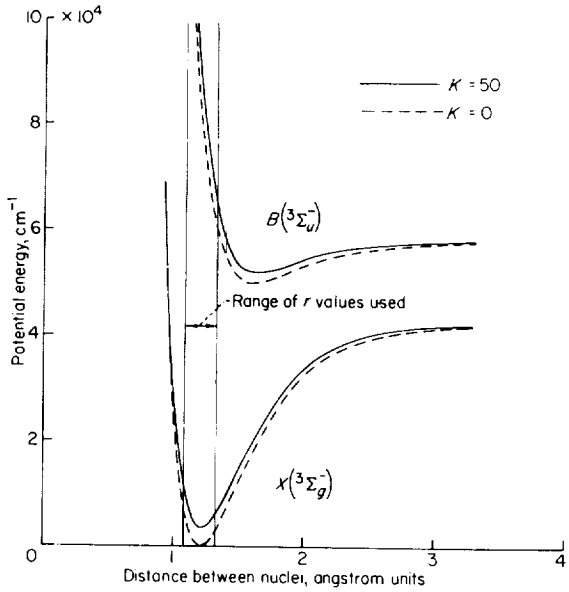

FIGURE 10.—Effect of rotation on potential curves.

X state). The minimum of the B state does not fall within the range of r values used. The vibrational energy eigenvalues and eigenfunctions are functions of the shape of the potential and thus are slightly different for each rotational state. These differences were neglected in using equation (3), since only eigenfunctions for the rotationless state were used in performing the calculations.

It should be pointed out that the effects of rotation on the potential curves were calculated for the worst conditions being considered, that is, at the highest temperature and at the extreme values of r. It is also important to note that, since both curves are affected in almost exactly the same way, the net distortion of the curves is what is really important and not the total energy shifts. In view of the fact that the actual potential curves are not accurately known, the approximately 2-percent energy shifts are not particularly serious. However, the 5-percent shift in the minimum of the lower curve may have an appreciable effect on the final results because it probably shifts the peaks of the lower-state wave functions by roughly comparable amounts.

A small amount of uncertainty is introduced into the energy change to be associated with a given transition when the rotational energy changes are ignored. The change in the rotational quantum number must be ± 1, which means that transitions differing in energy by twice the rotational level spacing in the upper state are counted to be the same. At $K=50$ two rotational level spacings in the B state amount to 164 cm^{-1}. This amounts to about 0.3 percent of a typical total energy change in a Schumann-Runge transition.

CALCULATION OF ABSORPTION COEFFICIENT USING THE REFLECTION OR DELTA FUNCTION METHOD

Calculation of initial-state wave functions.— The problem of evaluating the absorption coefficient was reduced in equation (3) to the problem of integrating the product of the vibrational wave functions for the initial and final states. For the continuum under study the initial states are bound vibrational levels of the $X(^3\Sigma_g^-)$ state. In this calculation they are represented by normalized Morse wave functions (refs. 22 and 23). These are solutions to Schrödinger's equation when a Morse potential is used for the vibrational potential. The following equations put these statements into mathematical form:

$$\frac{d^2\phi}{dr^2}+\frac{8\pi^2\mu}{h^2}[E''-V''(r)]\phi=0 \tag{5}$$

$$V''=D_e[1-e^{-\beta(r-r_e)}]^2 \tag{6}$$

$$\phi_{v''}(r)=\left[\frac{A_{v''}}{A_0}(x_e)^{v''}\right]\exp\left\{-\frac{1}{2}(x_e^{-1})\exp[-\beta(r-r_e)]-\left(\frac{1}{2}\right)(x_e^{-1}-2v''-1)\beta(r-r_e)\right\}Q_{v''} \tag{7}$$

The somewhat simpler harmonic oscillator wave functions (ref. 17, p. 76) could be used, but they neglect the asymmetry of the potential curve and this has an appreciable effect on the higher vibrational wave functions.

Figure 11 compares the Morse potential for the $X(^3\Sigma_g^-)$ state with the parabolic potential (corresponding to harmonic oscillator wave functions) and also with the Dunham (refs. 24 and 25), the Hulburt-Hirschfelder (ref. 26), and the Rydberg-Klein-Rees (discussed in refs. 27 and 28) potentials. Except for the parabolic potential the

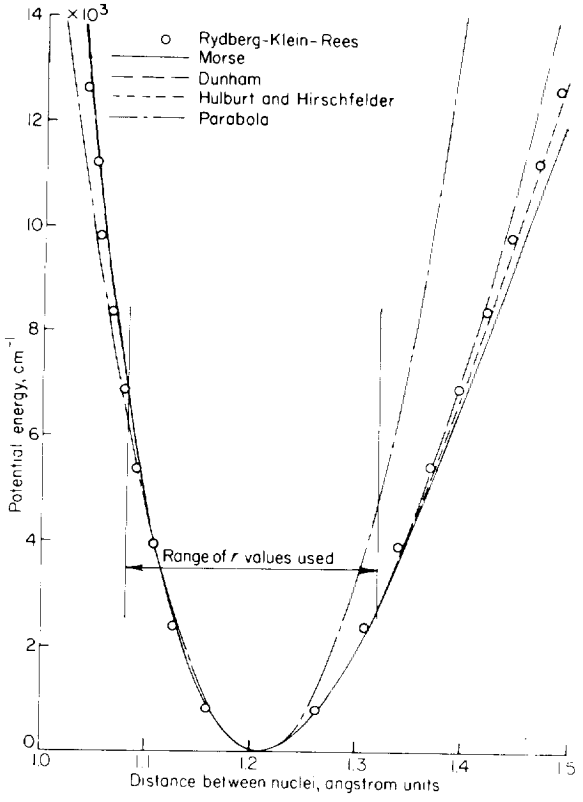

FIGURE 11. Comparison of potential curves for $X(^3\Sigma_g^-)$ state.

agreement is good over the range of r values needed (r= 1.08 to 1.32 angstrom units). The Morse potential was chosen not only because it appears to be a fairly good representation of the X state potential but also because, except for the parabolic potential, it is the only one mentioned which leads to solutions of the Schrödinger equation in closed form.

Substitution of delta functions for the final-state wave functions.—For the continuum under study the final state lies in a continuum of energy states above the dissociation limit of the $B(^3\Sigma_u^-)$ state and is represented by a wave function which near the turning point resembles a bound-state wave function. However, as r approaches infinity the wave function does not vanish but becomes a sine function, as is appropriate for the wave function representing a free particle. Good results can often be obtained by replacing this wave function by a delta function located at the turning point. This substitution is the basic assumption underlying the reflection method. Herzberg (ref. 17, p. 201) discusses why this method works. Briefly, it is successful because the main contribution to the overlap integral comes from the broad maximum near the turning point of the final-state wave function. Contributions from the other maximums and minimums tend to cancel each other so long as the oscillation frequency of the final-state wave function is large compared with the frequency of the initial-state wave function.

The Morse, Dunham, Hulburt-Hirschfelder, and Rydberg-Klein-Rees potentials for the B state are shown in figure 12. Also shown are a number of calculated points which indicate where the B state potential should lie in order to give agreement between the absorption coefficient predicted by the reflection method and the experimental data points shown in figure 2. The procedure used to obtain these points is described in appendix A.

The agreement among the three curves is not good. The data points show fairly good agreement among themselves even though they are based on three independent investigations and were obtained by two different methods of calculations. Because of this the true course of the potential is probably most nearly represented by a curve drawn through these points. The curve found in this way is shown in figure 13. A detailed

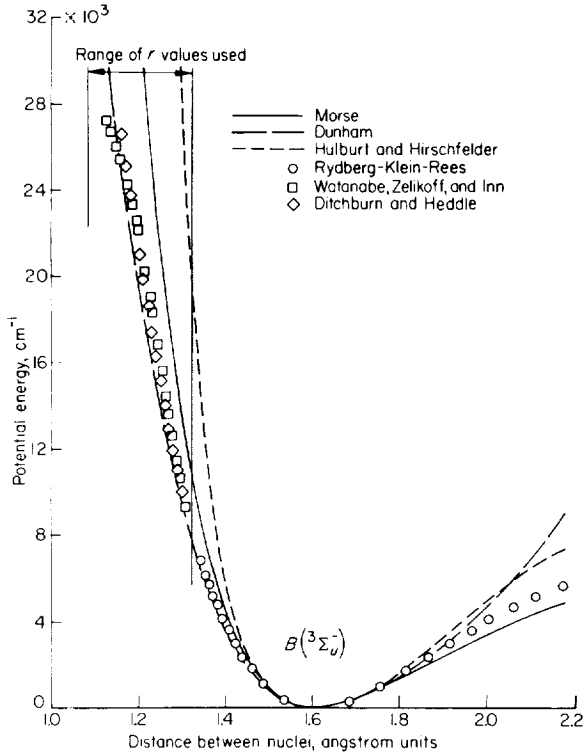

FIGURE 12.—Comparison of potential curves for $B(^3\Sigma_u^-)$ state.

discussion of the problem of accurately determining molecular potential curves from spectroscopic data is given by Coolidge, James, and Vernon (ref. 29). They do not deal directly with the determination of a curve above the dissociation limit, however.

Relation between energy of absorbed light quantum and internuclear distance at which transition occurs.—The energy difference between a given initial state and a given final state is the energy of the absorbed light quantum E^*. The value of r at the turning point of the upper state is uniquely related to the energy of the final state through the potential curve shown in figure 13. The energies of the discrete initial states were assumed to be the Morse eigenvalues for the X state. Thus, r_s and E^* were uniquely related for a given value of v''. The relation between r_s and E^* for $v''=0$ is shown in figure 14. In order to find the relation between r_s and E^* for $v''=1$, 2, and so forth, the energy difference between the level involved and the $v''=0$ level was subtracted from the E^* value found from the curve.

Procedure for calculating absorption coefficient by reflection method.—The procedure followed

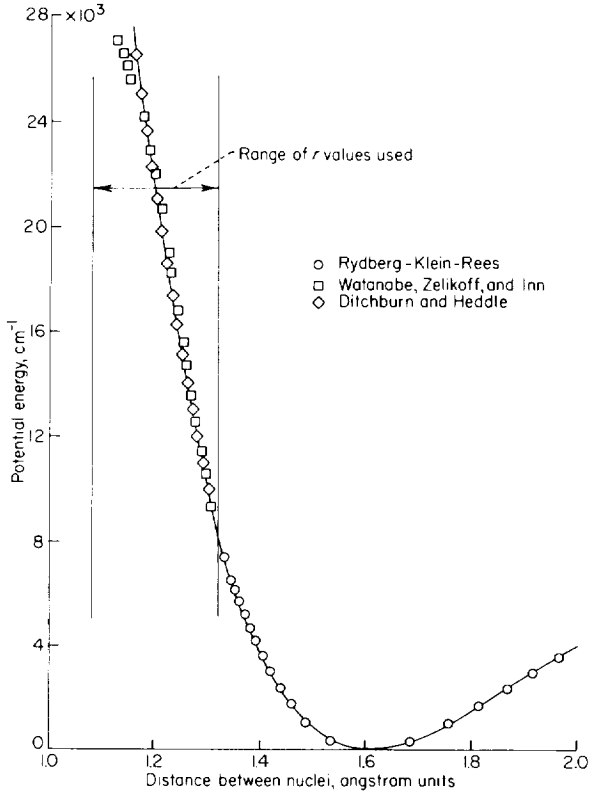

FIGURE 13.—Potential curve for $B(^3\Sigma_u^-)$ state used in calculations.

in using the reflection method to calculate the absorption coefficient was as follows:

(1) Morse wave functions were calculated for each of the 11 lowest vibrational levels of the X state. Some difficulty was encountered in evaluating the associated Laguerre polynomials of order four and greater because of the rapidly increasing number of decimal places required to obtain significant differences between the terms. This problem was solved by finding the roots of the polynomials and then expressing the polynomials in factored form.

(2) Equation (3) was used to calculate 11 $\hat{k}_{v''}(\lambda)$ curves, where $\hat{k}_{v''}(\lambda)=k_{v''}(\lambda)/k_0^m$. For these curves each of the 11 lowest vibrational levels of the X state was in turn considered to be the initial state in which absorption takes place. The upper-state wave functions were replaced by properly normalized delta functions located at the turning points. The following formula was the result:

$$\hat{k}_{v''}(\lambda)=\hat{k}_{v''}(r_s)=C_1\tilde{a}^{-1/3}E^*\phi_{v''}^2 \qquad (8)$$

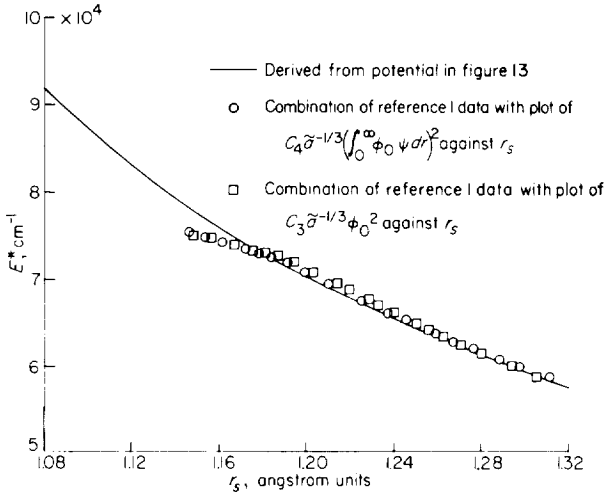

FIGURE 14.—Relation between E^* and r_s. (Curve is for $v''=0$. For higher vibrational levels subtract from E^* the difference in energy between $v''=0$ and $v''=v''$.)

where figure 14 was used to relate $\hat{k}_{v''}(\lambda)$ to $\hat{k}_{v''}(r_s)$ and C_1 was chosen to make the maximum value of $\hat{k}_0(\lambda)=1$. The derivation of this formula is given in appendix B. The $\hat{k}_{v''}(\lambda)$ curves obtained are shown in figure 15.

Some of the $\hat{k}_{v''}(\lambda)$ curves were not calculated over the entire range of wavelengths which is available in figure 15. The limits placed on the curves are indicated in the figure by vertical lines and correspond to the convergence limit of the band spectrum, that is, to the dissociation energy of oxygen in the B state. Note that the higher the initial vibrational energy level the farther the continuum extends toward longer wavelengths. Thus, the sharp division between continuum and band absorption which occurs at 1,750 angstrom units for oxygen at room temperature (ref. 18, p. 110) is not present at high temperature. Instead there is a region of overlapping band and continuum absorption beginning at 1,750 angstrom units and extending to longer wavelengths. New bands also appear as a result of the population of excited vibrational states of the X state. The wavelengths and relative intensities of the bands overlapping the continuum can be calculated by the Franck-Condon method but were not included in the calculations presented herein. Fraser, Jarmain, and Nicholls (ref. 30) have tabulated some of the transition probabilities and Treanor and Wurster (ref. 31) have observed some of the

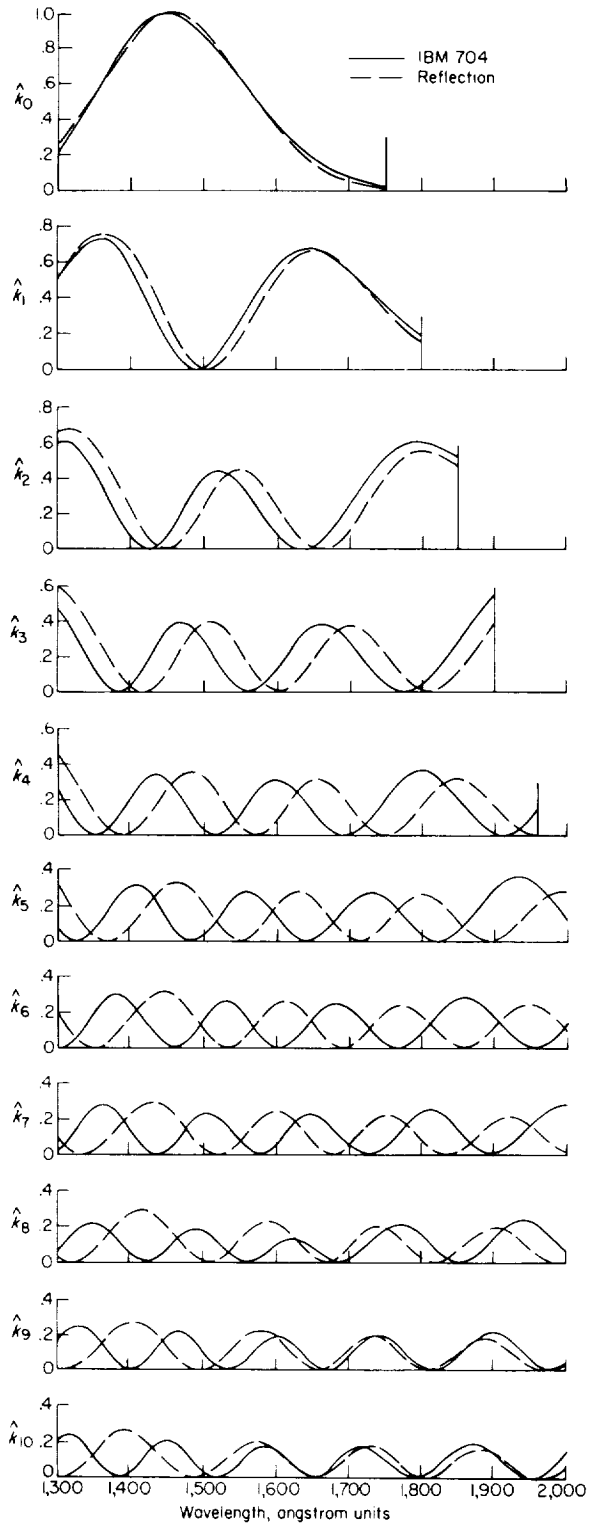

FIGURE 15. Absorption coefficient of oxygen molecules in each of the 11 lowest vibrational levels. Long-wavelength limit corresponds to dissociation energy of oxygen molecule.

bands. The extension of the continuum has been observed by Golden and Myerson (ref. 32).

(3) The overall absorption coefficient was calculated from the formula

$$\hat{k}_T(\lambda)=\sum N_{v''}(T)\hat{k}_{v''}(\lambda) \tag{9}$$

where $N_{v''}(T)$ is the weighting factor based on the equilibrium population of the initial vibrational levels. The curves obtained are shown in figure 16. The discontinuities correspond to the long-wavelength limits shown in figure 15. For figure 16 and all subsequent figures, complete equilibrium of the electronic states has been assumed unless otherwise noted.

Equation (9) neglects contributions to $\hat{k}_T(\lambda)$ from all initial states for which $v''>10$. About 1.8 percent of the oxygen molecules are in the $v''=10$ state at 10,000° K. Figure 15 shows that $\hat{k}_{10}(\lambda)$ oscillates somewhat like a sine function with a peak-to-peak amplitude of about 0.2. Thus, the average contribution of $\hat{k}_{10}(\lambda)$ to $\hat{k}_T(\lambda)$ at the highest temperature being considered is about 0.0018 with the actual contribution at a given wavelength varying from 0 to 0.0036. Contributions like this have a very small effect on the shape of the distribution curve. Contributions from the higher states are even smaller and are more or less randomly distributed over the wavelength range. Thus, stopping the calculations at $v''=10$ is believed to have a negligible effect on the shape of the distribution curve.

CALCULATION OF ABSORPTION COEFFICIENT USING A DIGITAL COMPUTER

Description of method and procedures.—As has already been mentioned, equation (3) reduces the problem of calculating the absorption coefficient to the evaluation of the vibrational overlap integral $\int_0^\infty \phi_{v''}\psi dr$. For the digital computer calculations Morse eigenfunctions were used for the ground-state wave functions and the excited-state wave functions were found by using the computer to solve the Schrödinger equation

$$\frac{d^2\psi}{dr^2}+\frac{8\pi^2\mu}{h^2}[E'-V'(r)]\psi=0 \tag{10}$$

The solution was started by specifying the values of ψ and $d\psi/dr$ at the turning point of the motion in the upper state and was continued by

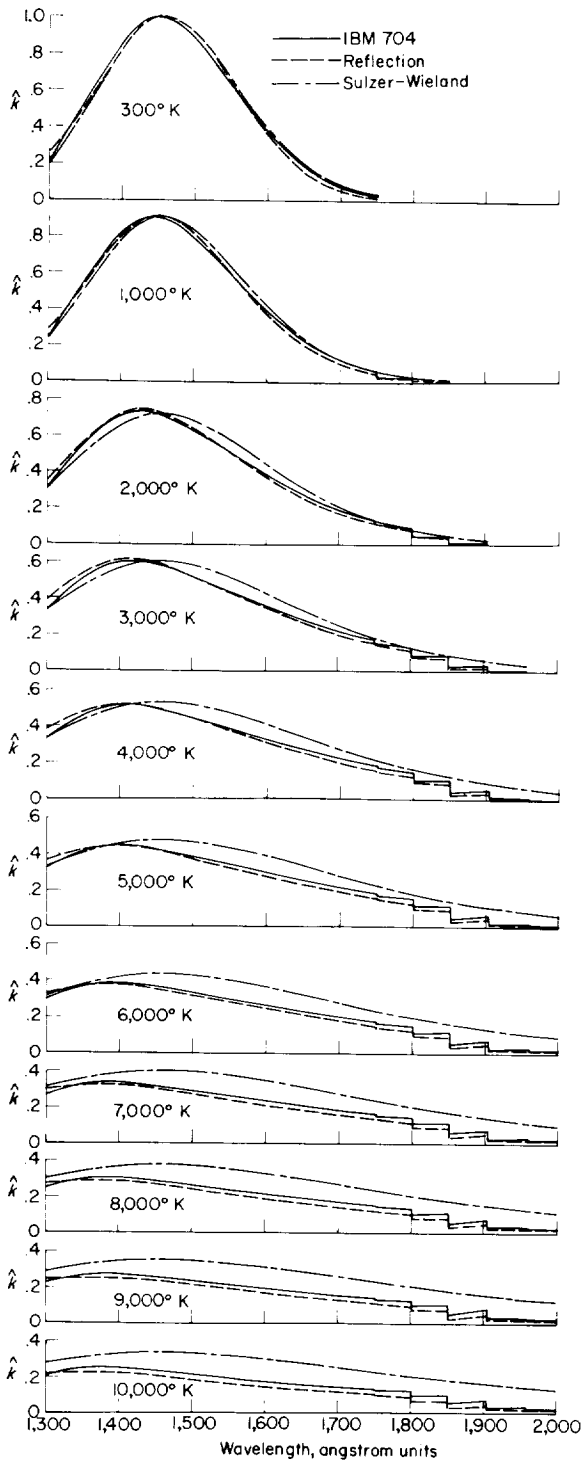

FIGURE 16.—Absorption coefficient of oxygen at temperatures from 300° to 10,000° K. Long-wavelength limit corresponds to that in figure 15.

the Runge-Kutta procedure (discussed in ref. 33, p. 469) as far as needed into the region where $(E'-V'')>0$. The machine evaluated the overlap integral at the same time and the result obtained at the end of the run was $\int_{r_s}^{\infty}\phi_{v''}\psi dr$, where r_s is the internuclear distance corresponding to the starting point. It was only necessary to integrate out to r values where the integral attained a constant value since the integrand vanishes when $\phi_{v''}$ vanishes. Runs were made in the opposite direction (that is, into the region where $(E'-V'')<0$) from the same starting point to evaluate $\int_{0}^{r_s}\phi_{v''}\psi dr$ and the two parts were added to obtain $\int_{0}^{\infty}\phi_{v''}\psi dr$. The machine results in the region where $(E'-V'')<0$ were not satisfactory. The trouble was due to the fact that $d^2\psi/dr^2>0$ in this region, and the solution is therefore unstable. Coolidge, James, and Present reported similar difficulty (ref. 19, p. 200). The problem could have been solved by adjusting $d\psi/dr$ at r_s slightly so as to obtain positive diverging and negative diverging ψ functions for nearly identical values of $d\psi/dr$ at r_s. However, the required integrals were computed instead with a desk integrator using Hankel functions for the ψ functions. Schiff points out that Hankel functions are solutions of equation (10) when V'' is a linear function of r (ref. 34, p. 182). The tangent to the potential curve was used for V'' in the Hankel solutions.

The following checks were made on the machine results:

(1) For a few runs Hankel solutions were computed over the whole range of r values necessary. The tangent to the potential curve was used for the potential function. The observed deviations from the machine-computed ψ functions were in the correct directions and vanished as the point of tangency was approached.

(2) Plots of the integrand were made over the range of r values used. The junction of the two parts at the starting point was smooth in every case.

(3) Spot checks of the value of $\int_{0}^{\infty}\phi_{v''}\psi dr$ were made with a desk integrator and were in satisfactory agreement with the machine results.

The numerical values of the vibrational overlap integrals are properly related to each other only when normalized wave functions are used. The Morse wave functions used were normalized but the ψ functions obtained from the computing

machine were not. The necessary normalization factor is shown in appendix C to be $F=(\text{Constant})(\tilde{a}^{-1/6}\tilde{E}^{1/4})$ where $\tilde{a}$ is the slope of the potential curve at r_s.

When F was substituted in equation (3) the result was

$$\hat{k}_{v''}(\lambda)=\hat{k}_{v''}(r_s)=C_2\tilde{a}^{-1/3}E^{*}\left(\int_0^{\infty}\phi_{v''}\psi dr\right)^2 \quad (11)$$

Equation (11) is comparable to equation (8) in the previous section on the reflection method. Figure 14 was used to relate $\hat{k}_{v''}(\lambda)$ to $\hat{k}_{v''}(r_s)$ and C_2 was chosen to make the peak value of $\hat{k}_0(\lambda)=1$.

Calculation of absorption coefficient from machine results.—The procedure followed in calculating the absorption coefficient was exactly the same as that used for the reflection method except that equation (11) was used to calculate the values of $\hat{k}_{v''}$ in place of equation (8). The $\hat{k}_{v''}(\lambda)$ curves are shown in figure 15 and the $\hat{k}_T(\lambda)$ curves are shown in figure 16.

CALCULATION OF ABSORPTION COEFFICIENT USING SULZER-WIELAND FORMULA

Statement of the formula and calculation of absorption coefficient.—The Sulzer-Wieland formula is written in terms of the wave number $\tilde{\nu}$ and is as follows (ref. 7, p. 664):

$$k_T(\tilde{\nu})=k_0'''[\tanh(\Theta/2T)]^{1/2}\exp\{-\tanh(\Theta/2T)[(\tilde{\nu}-\tilde{\nu}_m)/\Delta\tilde{\nu}_0]^2\} \quad (12)$$

where k_0''' is the maximum value of $k_T(\tilde{\nu})$ at 0° K, Θ is the characteristic temperature which appears in the vibrational partition function for the X state, $\tilde{\nu}_m$ is the wave number for which $k_T(\tilde{\nu})$ has its maximum value, and $\Delta\tilde{\nu}_0$ is the natural half breadth of the $k_0(\tilde{\nu})$ curve; that is, $\Delta\tilde{\nu}_0$ is the difference between the two values of $\tilde{\nu}$ for which $k_0(\tilde{\nu})=e^{-1}k_0'''$.

In order to use equation (12) k_0''', $\tilde{\nu}_m$, and $\Delta\tilde{\nu}_0$ must be evaluated from experimental measurements of the absorption at a temperature low enough so that $k_T(\tilde{\nu})$ is for all practical purposes identical to $k_0(\tilde{\nu})$. Room-temperature measurements are adequate for oxygen, since practically all oxygen molecules are in the lowest vibrational state at room temperature.

The following values were used for calculating the absorption coefficient for oxygen: $k_0'''=400$ cm^{-1}; $\tilde{\nu}_m=69{,}000$ cm^{-1}; $\Delta\tilde{\nu}_0=6{,}481$ cm^{-1}; and $\Theta=2{,}260°$ K. The resulting $\hat{k}_T(\lambda)$ curves are shown in figure 16.

Underlying assumptions and resulting limitations.—The assumptions underlying the Sulzer-Wieland formula are as follows:

(1) Harmonic oscillator wave functions (ref. 34, p. 64), which are solutions of Schrödinger's equation for a parabolic potential, were assumed for the initial-state functions.

(2) The upper-state potential was assumed to be a straight line.

(3) The upper-state eigenfunctions were replaced by delta functions as in the reflection method.

(4) The electronic transition probability was assumed to be independent of r.

(5) The expression $\int_0^{\infty}(k/\tilde{\nu})d\tilde{\nu}=\text{Constant}$ (ref. 7, p. 661, and ref. 17, p. 203) was replaced by $\int_0^{\infty}k d\tilde{\nu}=\text{Constant}$. This is equivalent to omitting E^{*} from equations (8) and (11).

(6) The effect of molecular rotation was neglected.

With the assumptions mentioned the calculation was simplified enough to permit summation of the equations over all the initial vibrational states to obtain the result given in equation (12). The result is symmetrical about $\tilde{\nu}_m$ and thus is incapable of showing any shift of the peak position with temperature such as appears in figure 1. Equation (12) is similar to the equation for the normal curve of error $y=(2\pi)^{-1/2}\exp(-x^2/2)$ since it can be written as $y=(\text{Constant})\exp(-\tanh ax^2)$ and the hyperbolic tangent does not differ much from its argument for small values of the argument.

The Sulzer-Wieland equation is applicable to any diatomic molecule for which the necessary constants can be evaluated and is formally applicable at any temperature. In practice, it has been found to agree well with measured absorption coefficients for the halogens at temperatures up to 2,000 K (figs. 3 and 4 and refs. 10 to 16). Because of the rather drastic assumptions made in order to simplify the theory enough to permit the result to be written in the form of a single simple equation, it is necessary to guard against using it without making some sort of evaluation of its probable range of validity for the molecule in question and for the temperature range needed. As discussed subsequently, the Sulzer-Wieland

formula is not adequate for calculation of the absorption coefficient of oxygen up to 10,000° K.

CALCULATION OF ABSORPTION COEFFICIENT INCLUDING AN EMPIRICAL CORRECTION FOR VARIATION OF ELECTRONIC TRANSITION PROBABILITY WITH INTERNUCLEAR DISTANCE

Determination and discussion of correction factor.—The discussion following equation (3) mentioned that an empirical evaluation of the variation of the electronic transition probability Ω with internuclear distance could be obtained by comparing experimental values of the absorption coefficient to theoretical values calculated from equation (3). Since the electronic transition probability was assumed to be constant in the calculations based on equation (3), the factor required to make theory agree with experiment at room temperature can be interpreted as being proportional to Ω.

Figure 17 shows the variation of Ω with wavelength. It was derived by comparing a smooth curve drawn through the experimental data with the digital-computer results. The variation is slow and smooth from 1,750 down to 1,375 angstrom units. At 1,375 angstrom units the slope suddenly changes sign and the factor drops sharply to zero at 1,300 angstrom units.

This sharp dropoff is particularly interesting and significant, since it indicates the presence of an additional factor affecting the absorption coefficient. Watanabe, Zelikoff, and Inn (ref. 1, p. 26) suggested that another potential interacts with the $B(^3\Sigma_u^-)$ potential to cause this disturbance. Evidence has been cited (refs. 35 to 37) for the existence of a potential in addition to the five well-established ones shown in figure 5. It is designated as $^3\Pi_u^-$ and perturbations between it and the $B(^3\Sigma_u^-)$ state are allowed by the selection rules

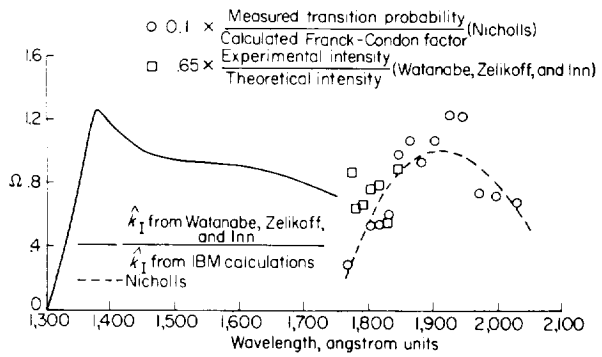

FIGURE 17.—Ratio of experimental to theoretical absorption coefficient at 300° K.

(ref. 17, p. 284). Figure 18 shows that the $^3\Pi_u$ curve which was proposed by Flory (ref. 35) and later substantiated by Volman (ref. 36) could be extrapolated to cross the $B(^3\Sigma_u^-)$ curve at the point required to cause the disturbance noted at 1,375 angstrom units. On the other hand, Wilkinson and Mulliken (ref. 37) gave some good arguments for believing that the $^3\Pi_u$ curve takes a different course. Their curve is also shown in figure 18. Vanderslice, Mason, and Maisch (ref. 28, p. 16) support Wilkinson and Mulliken and suggest that Flory's curve may correspond to a $^5\Sigma_u^-$ state. Perturbation of the $B(^3\Sigma_u^-)$ state by this state is also possible, since only the multiplicity selection rule is violated, and this is fairly common.

Nicholls reported a determination of the variation of Ω from the discrete part of the Schumann-Runge band spectrum (ref. 21, p. 750). His results, which are based on calculated Franck-Condon factors and absorption measurements by Ditchburn and Heddle (ref. 2), are shown in figure 17. Also shown are some additional points prepared from data given by Watanabe, Zelikoff, and Inn (ref. 1, p. 25).

Nicholls' curve does not join smoothly onto the curve derived from the continuum even when allowance is made for the scale difference between the curves in the figure. Possibly this could also be explained by interaction between potentials, since figure 18 shows Wilkinson and Mulliken's

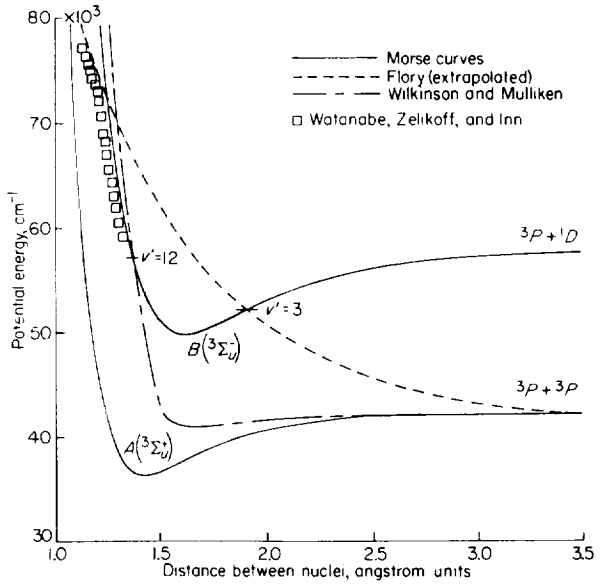

FIGURE 18.—Illustration of two suggested new potential curves for oxygen.

curve crossing the $B(^3\Sigma_u)$ curve near the point which corresponds to the dissociation limit of the Schumann-Runge band system. In any case the variation of Ω derived from the continuum is the appropriate one to use in calculating the correction factor for the continuous absorption.

Application of correction factor to calculation of absorption coefficient.—In the preceding section and in figure 17 Ω was treated as though it were a function of wavelength. Because λ and r_s are uniquely related for a given initial vibrational level, room-temperature data can be treated this way. At high temperature, however, several initial vibrational states are present and the fact that Ω is basically a function of r rather than λ must be kept in mind.

The empirical correction factor shown in figure 17 was plotted as a function of r_s and was applied to the $\hat{k}_{r'}(\lambda)$ curves of figure 15 by using the λ,r_s relations defined in the discussion of the reflection method. The new $\hat{k}_{r'}(\lambda)$ curves are not shown but the resulting new $\hat{k}_T(\lambda)$ curves for the digital-computer calculations are shown in figure 19.

EXPERIMENTAL DETERMINATION OF ABSORPTION COEFFICIENT

BACKGROUND MATERIAL

Statement of experimental problem.—The experimental problem was the determination at several selected wavelengths of the absorption coefficient k for molecular oxygen at temperatures up to 10,000° K. Since k is a function of wavelength and temperature these quantities had to be well defined during a measurement. The solution of equation (1) for the absorption coefficient

$$k=-(1/\hat{\rho}l)\log_e(J/J_o) \tag{13}$$

shows that the data necessary for the determination of k at given wavelength and temperature were the ratio of the emergent to incident light intensity, the reduced gas density, and the path length.

Problem of obtaining heated gas samples.—A direct approach to the problem of obtaining heated gas samples was made in references 7, 10, 11, and 12 by using electric heaters. A more novel, and for some purposes more satisfactory, way of heating the gas samples was used in references 9 and 13 to 16, where shock waves were used to compress

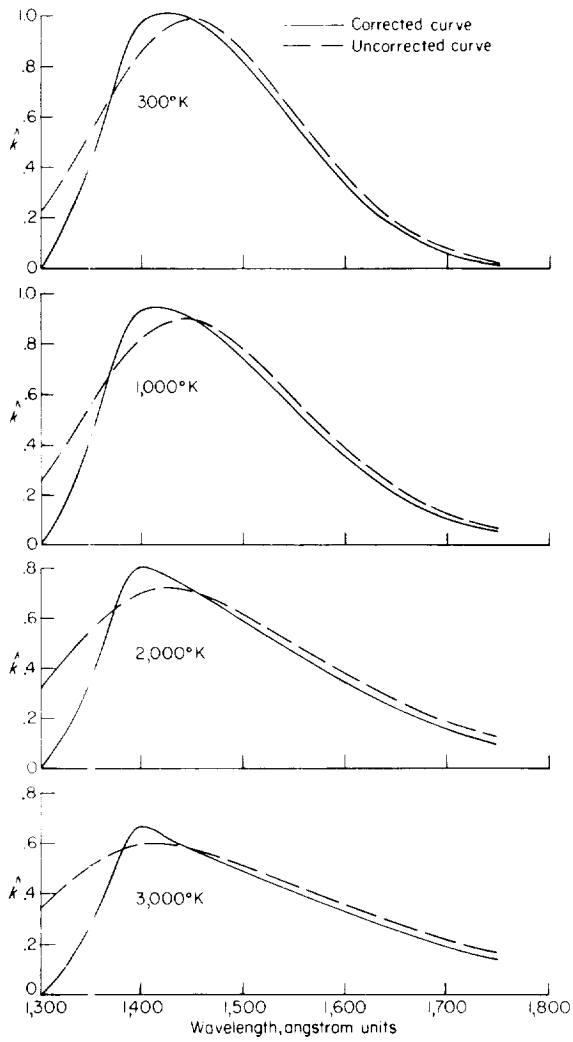

FIGURE 18. Corrected absorption coefficient of oxygen at temperatures from 300° to 10,000° K.

and heat the gases. Since molecular oxygen dissociates into atoms at temperatures above a few thousand degrees Kelvin, the almost instantaneous heating provided by the shock heating method was necessary for the study of the absorption of oxygen up to 10,000° K. Oxygen persists in the molecular form for a short time behind a shock front because more molecular collisions are required for dissociation of the oxygen molecule than for the excitation of its translational and rotational degrees of freedom (refs. 38 and 39).

The advantages of using shock waves to heat the gas samples were:

(1) The containing vessel was not appreciably heated. This was very important since the two

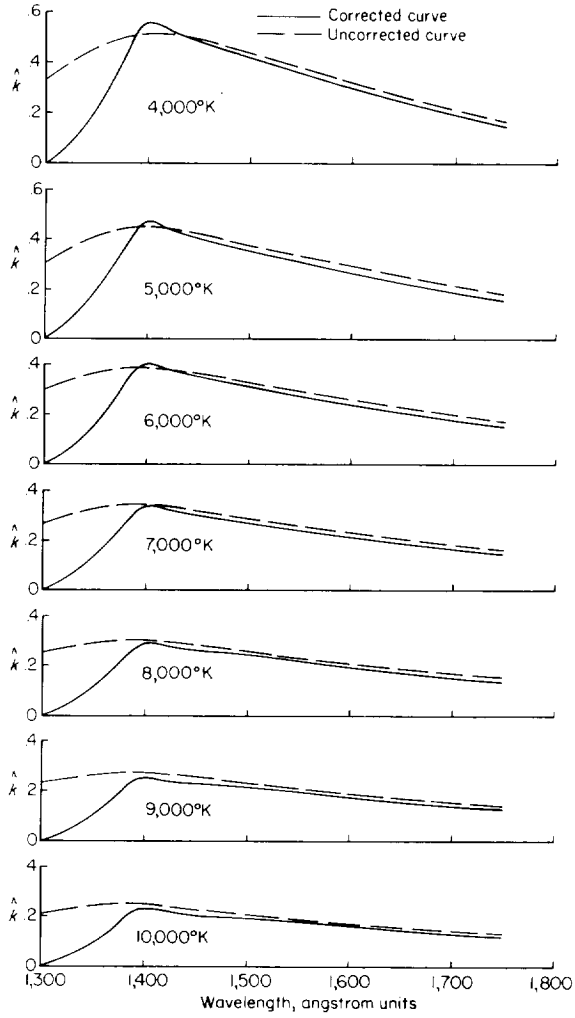

FIGURE 19.– Concluded.

materials which transmit light well in the vacuum ultraviolet, namely lithium fluoride and calcium fluoride, lose their transparency as the temperature increases (ref. 40) and break easily under the mechanical stresses imposed by temperature gradients (refs. 41 and 42). Even if these obstacles could have been overcome no containing walls would have long withstood temperatures up to 10,000° K, gas purity and high vacuum would have been difficult to maintain at high temperature, and temperature gradients between heat sources and surroundings would have caused considerable trouble.

(2) The intensity of the light source did not have to be steady since the transmitted light intensity changed at the shock front in a fraction of a microsecond.

(3) The temperature produced was uniform along the path length.

The disadvantages of using shock waves to heat the gas samples were:

(1) The temperature had to be calculated from the thermodynamic properties of the gas and the measured shock velocity.

(2) An intense ultraviolet source was required to maintain a useful signal-to-noise ratio in the fast-responding light detector required.

Adequate descriptions of the nature of shock tubes and their use in producing hot gas samples are given in the literature (refs. 43 to 47). Ideal shock-tube flow and many effects of gas imperfections have become common knowledge. However, a paper by Duff (ref. 48) deserves special mention because the conditions cited are precisely those present in the shock tube used for the work reported herein. Before the paper appeared the following puzzling facts had been noted: The distance between the shock front and the contact surface between driven and driver gases was noticed to be far shorter than that predicted by shock-tube theory. It was also noticed that this distance, which measures the length of the hot gas region behind the shock front, did not increase as the shock wave progressed down the tube. This also conflicted with the usual shock-tube theory. Both of these effects were reported by Duff and were attributed along with certain other effects to the formation of a laminar boundary layer behind the shock front. While this disturbance to the otherwise easily calculated thermodynamic properties in the hot flow region complicates the task of those interested in studying relaxation rates behind shock waves, it does not affect the thermodynamic calculation of temperature and density immediately behind the front, and these are the only properties required in this investigation.

Problems peculiar to vacuum ultraviolet spectral region.—Spectral measurements at wavelengths shorter than about 2,000 angstrom units are considerably more difficult than they would be in the visible spectrum because of the following items:

(1) There are only a few materials which are transparent in the vacuum ultraviolet region (ref. 49). Quartz becomes opaque at about 1,500 angstrom units, sapphire at about 1,425 angstrom units, barium fluoride at about 1,350 angstrom units, calcium fluoride at about 1.225

angstrom units, and lithium fluoride at about 1,050 angstrom units. At wavelengths shorter than 1,050 angstrom units no windows, prisms, or lenses are available. Quartz and sapphire are strong materials and will withstand much thermal and mechanical stress, but calcium fluoride and lithium fluoride are very susceptible to both thermal and mechanical stresses (ref. 42, p. 740).

(2) The contamination of the surfaces of mirrors, gratings, lenses, and windows by even thin films of oil, water, or other substances often results in a great reduction in efficiency in this spectral range (refs. 50 and 51).

(3) Since the oxygen present in air absorbs light strongly in this spectral region, all light paths must be kept free from oxygen, either by providing an evacuated enclosure or by using nonabsorbing gases in the light paths.

(4) Sources of intense ultraviolet light in the spectral range from 1,300 to 1,750 angstrom units are still in the development stage. In the past the most commonly used sources for studying spectra in the region were as follows:

(a) The positive column discharge in hydrogen (refs. 52 and 53), which produces a continuum from 1,650 angstrom units upwards and the many-line molecular hydrogen spectrum below 1,650 angstrom units.

(b) The continua emitted by the rare gases xenon and krypton under microwave excitation (refs. 54 and 55). Xenon emits from 1,470 angstrom units upwards, with peak emission near 1,750 angstrom units. Krypton emits from 1,236 angstrom units upwards, with peak emission near 1,500 angstrom units.

(c) The Lyman continuum (discussed in ref. 54, p. 344, and refs. 56 and 57) produced by a violent condenser discharge through a narrow-bore tube. This source emits a continuum running from a few hundred angstrom units upwards.

Conventional designs of the first two types mentioned failed to produce adequate intensity of ultraviolet light. The Lyman source tried produced intense ultraviolet light, but the material ejected quickly ruined the lithium fluoride window on the shock tube. References 58 to 62 discuss some other light sources for the vacuum ultraviolet. All these were judged to be unsatisfactory for the purposes of this investigation. The search for a suitable light source was the greatest obstacle encountered in preparing the experimental equipment. However, suitable sources were finally developed. Since these sources have not been thoroughly investigated, they probably are not optimum designs. The sources used are described in the section entitled "Description of Equipment."

Light-detection problems.—A fast-responding detector for ultraviolet light was necessary in order to take advantage of the fact that molecular oxygen persists for a short time behind a shock front. Photoelectric detection using a photomultiplier tube was the only solution found.

Since the glass envelope of a photomultiplier tube does not transmit light in the vacuum ultraviolet, a coating of sodium salicylate was applied to the glass in front of the light-sensitive area. Sodium salicylate fluoresces with uniform quantum efficiency (ref. 1, p. 17, and ref. 63) over the entire range of wavelengths needed (1,300 to 1,750 angstrom units). The peak of the emitted light (λ=4,100 angstrom units) is close to the sensitivity peak of an S-11 photoelectric surface (λ=4,400 angstrom units), which was the type used.

No information was available in the literature on the fluorescence decay time of sodium salicylate, but the experience gained in this investigation and in that reported in reference 39 indicates that it is less than 10^{-7} second. The rise time of the signal obtained by coating an RCA 1P21 photomultiplier with some other organic phosphors was measured in reference 64 and was found to be of the order of 10^{-8} second.

DESCRIPTION OF EQUIPMENT

Basic items.—In simplest terms the equipment items needed to measure the absorption coefficient of a sample of gas are a light source, an absorption path of known length, a device to select light of a known wavelength (i.e., a monochromator), and a light detector. The absorption path is in the shock tube; the description given includes all information pertaining to the shock tube, such as, shock-velocity measuring equipment and operation of the shock tube. The description given of the light detector includes information pertaining to the recording as well as to the detection of the light signal. Figure 20 illustrates the main items of equipment and how they are related to each other.

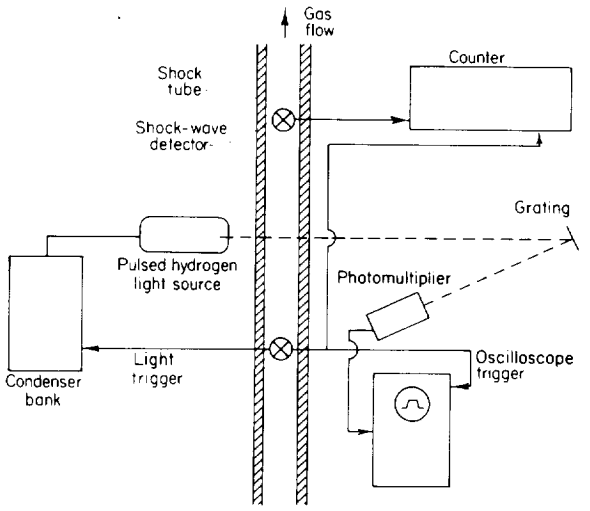

FIGURE 20. Schematic diagram of equipment.

Detailed descriptions.—As has already been mentioned, the ultraviolet light sources used were developed at the Langley Research Center. They are best described as pulsed hydrogen discharge lamps. Figure 21 is a drawing of the first successful lamp built. As indicated in the figure, the cathode and most of the glass envelope were taken from a radio transmitter tube (RCA type 872A). The original intention was to operate it as a hot cathode, continuously operating, hydrogen discharge lamp. While the usual continuum and many-lined molecular spectrum were obtained this way, the intensity was inadequate. When a condenser was discharged through the tube, however, intense ultraviolet light was observed. After a moderate development program, the following combination of parts was found to give satisfactory results over at least a portion of the desired spectral range (1,550 to 1,750 angstrom units):

(1) The lamp as shown in figure 21. The cathode was no longer heated but was merely used as an electrode.

(2) An energy source capable of producing a current pulse of 2,000 amperes for 100 microseconds. An artificial transmission line made up of twenty 2-microfarad, 4-kilovolt condensers, and ten 5-microhenry, center-tapped coils connected as shown in figure 22 was used for this purpose. The condensers in the artificial transmission line were charged to about 4 kilovolts. A noninductive series resistance of 0.8 ohm was included to match the load impedance to the output impedance of the line.

(3) An electronic switch. A Kuthe Laboratories hydrogen thyratron tube (Type 5948/1754), rated at 1,000 amperes peak current and 25 kilovolts peak voltage, was used. It applied the voltage to the discharge lamp less than 1 microsecond after being triggered.

(4) A tank of commercial-grade hydrogen. This gas was allowed to flow slowly through the discharge tube. The hydrogen pressure was maintained in the discharge region at about 1 millimeter of mercury by continuous pumping.

Figure 23 shows the measured light intensity distribution with wavelength for this light source.

One other light source from the many tried is shown in figure 24. It was used for the shorter wavelengths where the light intensity produced by the first source was low. The intensity dis-

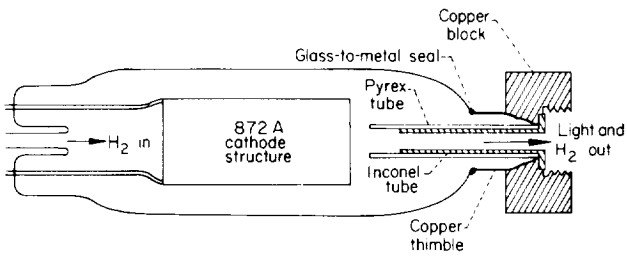

FIGURE 21. Light source used for wavelength range 1,550 to 1,750 angstrom units.

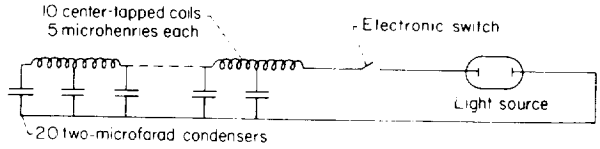

FIGURE 22. Artificial transmission line used for energy storage.

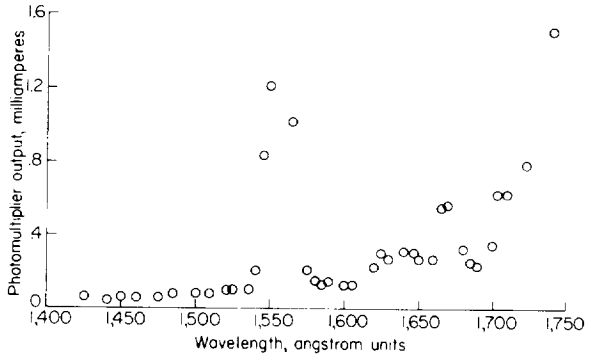

FIGURE 23. Measured light intensity distribution for source made from RCA type 872A transmitter tube.

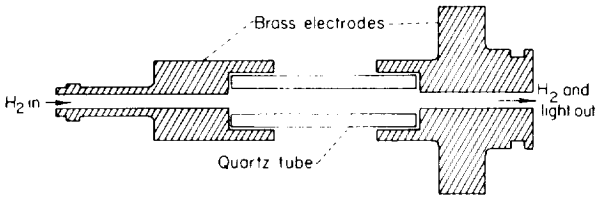

FIGURE 24.- Light source used for wavelength range 1,300 to 1,500 angstrom units.

tribution with wavelength for this lamp was essentially the same as that for the first source but, due to the confinement of the discharge to a smaller space, the intensity was higher.

A pulsed hydrogen discharge lamp was also used by Camac, Camm, and Petty (ref. 39). According to a communication from Dr. Morton Camac of the AVCO Corporation this lamp has two hollow cylindrical electrodes spaced about ½ inch apart and sealed in a glass tube containing hydrogen at several millimeters of pressure. The hydrogen supply was maintained by a small amount of uranium hydride (ref. 62), which also served as a getter material to remove residual impurities. Ultraviolet light from the molecular hydrogen spectrum was produced when the lamp was flashed at about 500 volts and the light left the tube through a calcium fluoride window.

Another flash-type ultraviolet source similar to those developed at the Langley Research Center was reported by Golden and Myerson (ref. 65). Light was produced in this lamp by discharging 120 joules through xenon, argon, or krypton contained in a 4-millimeter quartz capillary 15 centimeters long. Continuous emission was reported from 6,800 to 1,500 angstrom units. The photomultiplier output was 1 volt at 1,700 angstrom units using a circuit whose response time was less than 1 microsecond. This magnitude of signal is about the same as that obtained in the present investigation.

The absorption path was 1 inch long. This dimension was determined by the inside diameter of the stainless-steel tube used for the low-pressure section of the shock tube. Lithium fluoride windows ⅛ inch in diameter and approximately 0.5 millimeter thick were set flush with the walls of the tube to permit the light to pass through perpendicular to the direction of motion of the shock wave. Both windows were masked to give apertures 1 millimeter wide by 3 millimeters high. The windows were cemented to the ends of removable plugs so that they could be frequently replaced. They were never polished nor cleaned in any way. Replacement windows were always freshly cleaved from a ⅛-inch-diameter core of lithium fluoride. After they were cemented in place the edges were smoothed flush with the metal and they were ready to be used.

The shock tube has been described by Schexnayder (ref. 66). It has two driver sections and a 16-to-1 area contraction just before the second diaphragm. The high-pressure chamber was filled with helium or hydrogen to about 100 atmospheres and the middle chamber was filled with helium to pressures ranging from ¼ to 1 atmosphere. The high-pressure diaphragms were 1/16-inch-thick steel plates; two saw cuts about eleven thousandths of an inch deep were cut on each plate in the shape of an X to promote easy tearing of the metal and so that the remaining flaps would flatten against the walls out of the way of the flowing gas. Both Mylar film and scribed brass shim stock were used for the second diaphragm. Sometimes the second diaphragm was omitted in order to work in a lower range of shock strengths. In this case the middle-chamber gas was the same as the gas under study.

Operation of the shock tube was initiated by building up the pressure in the high-pressure chamber until the steel diaphragm ruptured. The shock wave produced in the middle chamber broke the second diaphragm and reflected from the area contraction. The resulting region of hot, compressed, and essentially motionless gas served as the driver gas for the remainder of the shock tube.

The pressure in the 1-inch-diameter portion of the shock tube was always determined by the partial pressure of oxygen necessary to give a convenient amount of ultraviolet light absorption. At 1,550 angstrom units in oxygen this pressure was about 0.3 millimeter of mercury and at the same wavelength in a mixture of 10 percent oxygen in argon it was about 3 millimeters. The low-pressure section was always pumped to 20 microns of mercury before filling and was raised to the desired initial pressure by admitting the gas mixture through a leak valve while continuing the pumping. Thus, the tests were made in a slowly flowing gas. The effects of residual vapor pressures and small air leaks were minimized by this procedure. The leak rate of the shock tube when

closed off from the pump was 1 or 2 microns per minute.

The data necessary for the determination of the state of the test gas were:

(1) The initial gas temperature. This was taken to be the same as the temperature of the shock-tube wall and was measured to $\pm 1°$ K with a mercury-in-glass thermometer.

(2) The initial gas pressure. This was measured to ± 0.02 millimeter by two gages, an Alphatron vacuum gage and a 5-millimeter Hg dial gage. Both gages were calibrated against a McLeod gage and always agreed well with each other.

(3) The composition of the gas. Tank oxygen which was guaranteed 99.6 percent pure was used for the runs in pure oxygen. The percentage of oxygen in the mixture was measured to be 10.07 ± 0.10 percent. A tank of dry air was used for the runs in air. All gases were passed through an activated alumina filter at tank pressure before entering the shock tube.

(4) The velocity of the shock wave. This was measured by recording the time interval between signals received from ionization probes (ref. 67) located 5 inches in front of and 5 inches behind the absorption windows. These probes sensed the small amount of ionization associated with the shock fronts. The probe signals were applied to the grids of type 2D21 thyratron tubes as shown in the circuit diagram in figure 25. The pulses produced by the thyratrons were fed into a Berkeley counter which recorded the time interval between the pulses to ± 1 microsecond. The pulse from the first thyratron also triggered the light flash and the horizontal sweep of the Tektronix Type 545 oscilloscope used to display the photomultiplier signal. The ionization probes proved to be unreliable for detecting shock waves which produced temperatures below about 4,000° K. An attempt was made to obtain data at lower temperatures by using the ionization probes as glow discharge probes in the manner described by Lundquist (ref. 68). This effort was foiled by premature triggering of the thyratron tube associated with the second probe. The trouble was caused by interference produced by the heavy current discharge through the light source. Since lagging adjustment of the vibrational degree of freedom of oxygen would invalidate most, if not all, of the runs below 4,000° K, the effort was abandoned.

A grating monochromator was used to select a narrow band of wavelengths centered on the wavelength at which the absorption coefficient was to be measured. The monochromator was designed and constructed at the Langley Research Center. It was similar to the instrument described by Parkinson and Williams (ref. 69) and, like theirs, the output wavelength was varied by rotating the grating rather than sliding it along the Rowland circle. The diagram and equation shown in figure 26 give the essential design information.

The 2-inch-diameter aluminum-on-glass grating had a radius of curvature of 39.888 ± 0.008 centimeters. It was ruled at 15,000 lines per inch over an area of 1 by ¾ inch. It was blazed to concentrate most of the light in the first-order diffraction pattern. The dispersion was 0.0232 millimeter per angstrom over the wavelength range used.

Both the entrance slit and the exit slit were located 2 inches off the center line and at fixed but unequal distances from the axis of rotation of the grating. The design wavelength was 1,590 angstrom units. The corresponding values of x_1

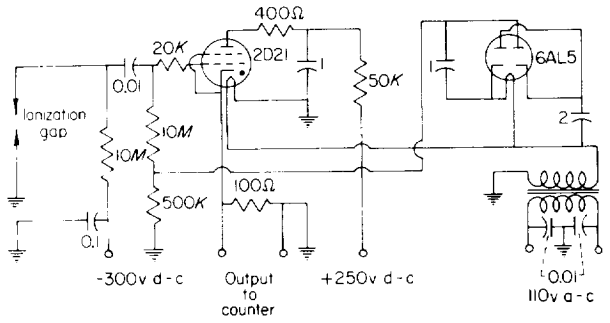

FIGURE 25.—Single pulse generator triggered by ion probe.

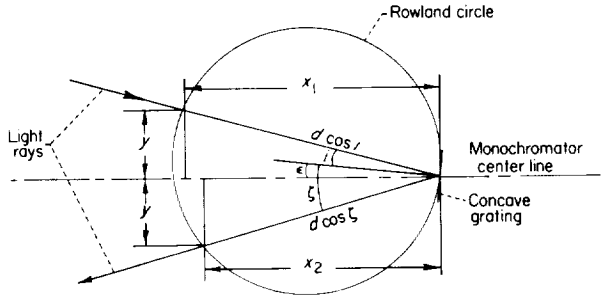

FIGURE 26.—Design diagram for ultraviolet monochromator. x_1,y, entrance slit position; x_2,y, exit slit position; $n\lambda = s(\sin\zeta - \sin i)$.

and x_2 were 15.524 and 15.331 inches, respectively. At 1,590 angstrom units the image of the entrance slit was focused on the exit slit. When the grating was rotated from the design position the values of x_1 and x_2 mentioned were no longer correct, and the image falling on the exit slit was out of focus. Since the defocusing was small over the wavelength range of interest and since photomultiplier detection does not require a sharp image, the only important effect was a shift of the central wavelength of the transmitted band by about 1 angstrom unit at the limits of the desired wavelength range.

The widths of the entrance and exit slits were both set at 0.010 inch. For equal slit widths the intensity distribution of transmitted wavelengths out of a continuum of uniform intensity is triangular in shape. The apex of the triangle represents maximum transmitted intensity and occurs at the central wavelength. For the slit settings mentioned the intensity dropped to one-half the maximum value at the central wavelength ± 5.5 angstrom units and to zero at the central wavelength ± 11 angstrom units.

Selection of a desired wavelength was accomplished by means of a calibrated micrometer screw which moved an arm attached to the grating. The screw was calibrated in terms of wavelength using lines from the spectrum of mercury down to 1,849 angstrom units and the resonance line of xenon at 1,470 angstrom units. The calibration points showed excellent agreement with a straight line drawn through the points.

In order to avoid absorption of the ultraviolet light by the oxygen present in air the monochromator was built in a vacuum-tight enclosure which was maintained at a pressure of 1 micron or less. To illustrate the importance of maintaining such a low pressure consider the calculated absorption at 1,450 angstrom units in the approximately 45 inches of light path between the shock tube and the photomultiplier. At 1 micron, 3 percent of the light was absorbed, at 10 microns, 12 percent, and at 100 microns, 72 percent.

A Dumont Type 6292 photomultiplier sensitized for ultraviolet by a coating of sodium salicylate was mounted about an inch from the exit slit of the monochromator. The glass envelope was in vacuum; the base was in air. The vacuum seal was made by means of a neoprene "O" ring at the juncture of the glass envelope and the base. The rise time of the photomultiplier output circuit was about 2×10^{-7} seconds and the rise time of the Tektronix Type 545 oscilloscope used to record the light signal was 10^{-8} seconds. The transit time of the shock wave across the light path was 2×10^{-7} seconds to 5×10^{-7} seconds, depending on the shock velocity. The linearity of the output current as a function of illumination was examined using data published by the manufacturer (ref. 70). The voltage was usually set at 150 volts per stage except for the potential between the cathode and the first dynode which was made twice as high as the interdynode potentials. The signal current was of the order of 2 milliamperes and the voltage divider current was about 6 milliamperes. The last two dynode stages were bypassed to avoid degeneration due to the signal current flowing in the divider. Linearity was better than 1 percent.

The uniform quantum efficiency of sodium salicylate as a function of wavelength and the belief that its fluorescence lifetime is short enough to permit its use as described above have already been mentioned.

The light intensity as a function of time was displayed on the screen of the oscilloscope and was photographed by a Polaroid Land camera. Figure 27 shows four typical records. The traces labeled "Vacuum" show the intensity obtained with vacuum in the shock tube; the traces labeled "Initial pressure" show the intensity obtained with the test gas at pressure p_1. The traces labeled "Record" correspond to those marked "Initial pressure" but show the shock wave passing through the absorption path. The traces labeled "Scattered light" were taken with the monochromator filled with air so that an estimate could be obtained of the amount of scattered light passing through the monochromator.

The hot gases behind strong shock waves are known to emit visible light and hot oxygen may emit some ultraviolet light also. However, no trace of emitted light was observed on any of the occasional runs for which the ultraviolet light source failed to operate properly.

DATA ANALYSIS

Data needed.—Equation (13) showed that the data needed to determine the absorption coefficient at given temperature and wavelength were the ratio of emergent to incident light intensity

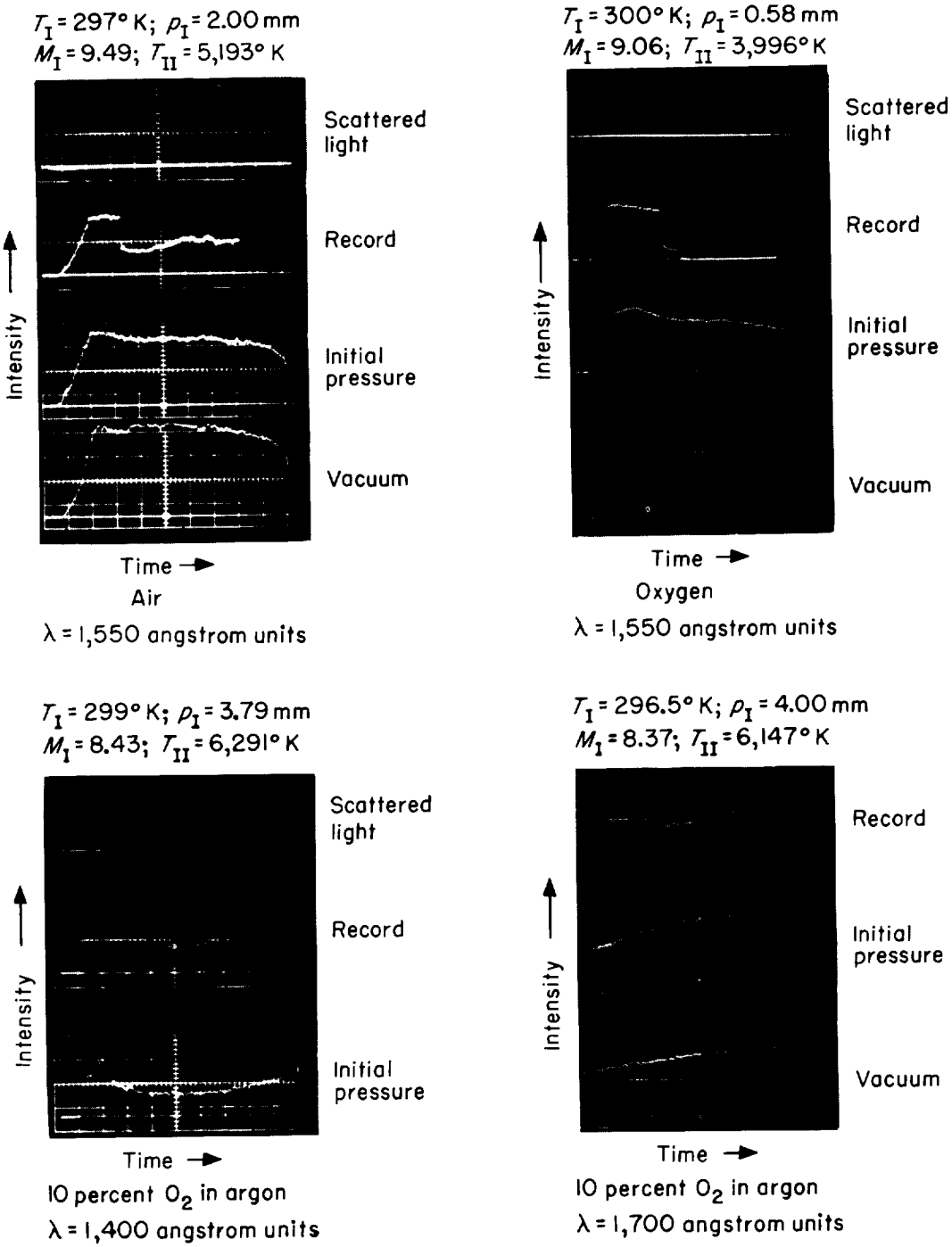

FIGURE 27. Typical shock-tube records. Time base on all records is 10 microseconds per centimeter.

immediately behind the shock front and the corresponding product of reduced gas density and absorption path length.

Description of analysis methods.—The diagram in figure 28 illustrates the measurements made on the oscilloscope records. The intensity J_o was the intensity which would have been observed if there had been no absorption of ultraviolet light in the shock tube. Because of the lack of reproducibility in the intensity of the source from one flash to another, the value of J_o obtained from the trace corresponding to vacuum in the shock

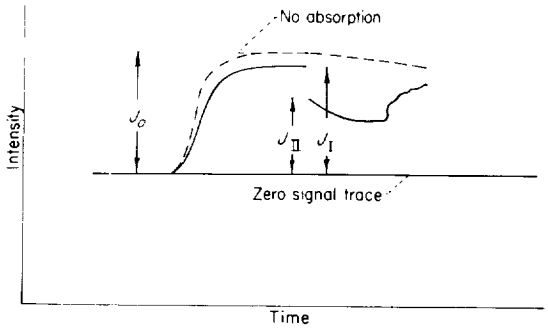

FIGURE 28.—Diagram illustrating measurements made on records.

tube was inaccurate. The following equations were set up so that J_o would not be required:

$$J_I/J_o=\exp\ (-k_I\hat{\rho}_I l)$$

$$J_{II}/J_o=\exp\ (-k_{II}\hat{\rho}_{II} l)=\exp\ (-k_{II}\sigma\hat{\rho}_I l)$$

$$J_{II}/J_o=(J_{II}/J_I)\ (J_I/J_o)=(J_{II}/J_I)\ \exp\ (-k_I\hat{\rho}_I l)$$

$$k_{II}=-(1/\sigma\hat{\rho}_I l)\ [\log_e\ (J_{II}/J_I)-k_I\hat{\rho}_I l]$$

Finally,

$$\hat{k}_{II}=(1/\sigma)\left[\hat{k}_I-\frac{\log_e\ (J_{II}/J_I)}{k_0^m\hat{\rho}_I l}\right] \tag{14}$$

The quantities required for the evaluation of the high-temperature absorption coefficient $\hat{k}_{II}$ from equation (14) were:

(1) The shock density ratio, $\sigma=\rho_{II}/\rho_I$
(2) The room-temperature absorption coefficient, $\hat{k}_I$
(3) The maximum value of $k_T(\lambda)$ at 0° K, k_0^m
(4) The light-intensity ratio across the shock, J_{II}/J_I
(5) The ratio of the initial oxygen concentration to the concentration of oxygen in the gas at 273° K and 1 atmosphere pressure, $\hat{\rho}_I$
(6) The absorption path length, l

Values for $\hat{k}_I$ were obtained from the corrected IBM calculations shown in figure 19. The intensities J_I and J_{II} were taken to be proportional to the distance of the signal trace from the zero signal trace on photographic enlargements of the original records. These distances were of the order of 10 to 50 millimeters ± 0.5 millimeter. Except for the absorption path length, $l=2.54\ \pm 0.1$ centimeters, the remaining items to be evaluated were σ, T_{II}, and $\hat{\rho}_I$.

The density and temperature behind a normal shock wave can be calculated from a knowledge of the shock velocity and the thermodynamic properties of the gas. The following conservation equations and the equation of state are the starting point:

(1) Conservation of energy,

$$\eta_I(p_I/\rho_I)+\frac{1}{2}u_I^2=\eta_{II}(p_{II}/\rho_{II})+\frac{1}{2}u_{II}^2 \tag{15}$$

(2) Conservation of momentum,

$$p_I+\rho_I u_I^2=p_{II}+\rho_{II}u_{II}^2 \tag{16}$$

(3) Conservation of mass,

$$\rho_I u_I=\rho_{II}u_{II} \tag{17}$$

(4) Equation of state,

$$p=\rho RT(1+\alpha) \tag{18}$$

From these equations the following expressions were found:

$$\overline{M}_{II}=\left(\frac{1}{2\eta_{II}-1}\right)\left[\frac{(1+\gamma_I M_I^2)\eta_{II}}{\gamma_I M_I}\right]-\left(\frac{1}{2\eta_{II}-1}\right)\left\{\left[\frac{(1+\gamma_I M_I^2)\eta_{II}}{\gamma_I M_I}\right]^2-(2\eta_{II}-1)\left[M_I^2+\frac{2}{\gamma_I-1}\right]\right\}^{1/2} \tag{19}$$

$$\sigma=\rho_{II}/\rho_I=M_I/\overline{M}_{II} \tag{20}$$

$$\frac{(1+\alpha)T_{II}}{T_I}=\gamma_I\overline{M}_{II}\left[\left(\frac{1+\gamma_I M_I^2}{\gamma_I M_I}\right)-\overline{M}_{II}\right] \tag{21}$$

Equation (21) was solved for $\overline{M}_{II}$ as follows:

$$\overline{M}_{II}=\frac{1+\gamma_I M_I^2}{2\gamma_I M_I}-\left[\left(\frac{1+\gamma_I M_I^2}{2\gamma_I M_I}\right)^2-\frac{(1+\alpha)T_{II}}{\gamma_I T_I}\right]^{1/2} \tag{22}$$

A graphical solution was obtained by plotting equations (19) and (22) against T_{II} at a constant value of M_I. Corresponding values of $\overline{M}_{II}$ and T_{II} were then read off the plots at the intersections of curves of equal M_I. Cross plots of T_{II} and σ as functions of M_I at a constant value of α were made from the results and some typical plots are shown in figures 29 and 30.

The three gas mixtures used were air, oxygen, and a mixture of 10-percent oxygen in argon. Calculations of T_{II} and σ for some of these mixtures have been published in references 71 and

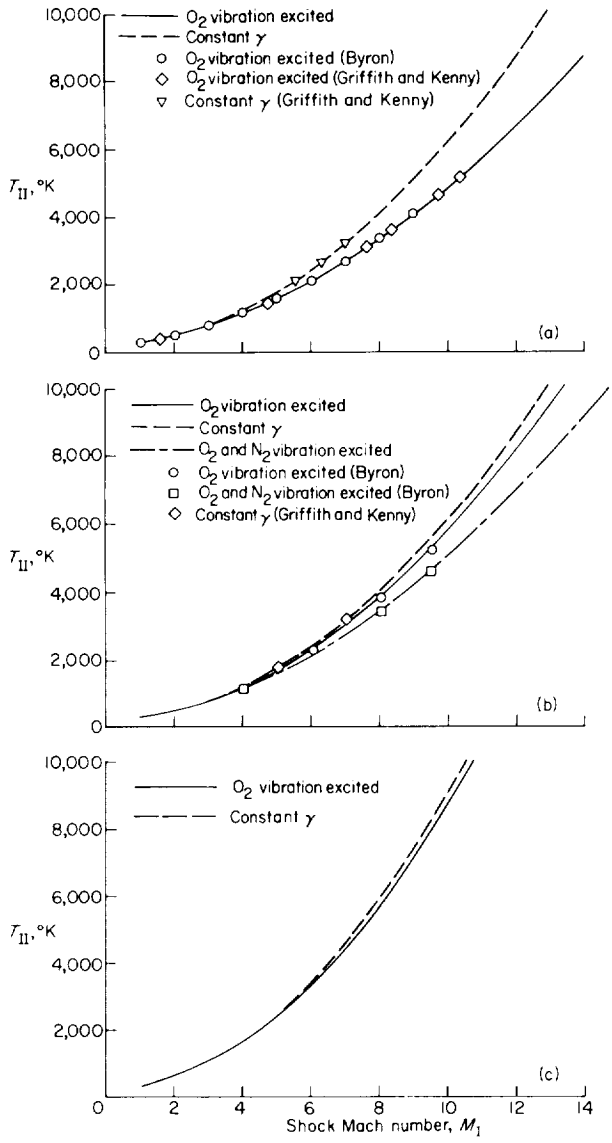

(a) Oxygen.
(b) Air.
(c) 10 percent O_2 in argon.

FIGURE 29.—Calculated values of temperature behind shock fronts. $T_1 = 300°$ K; $\alpha = 0$.

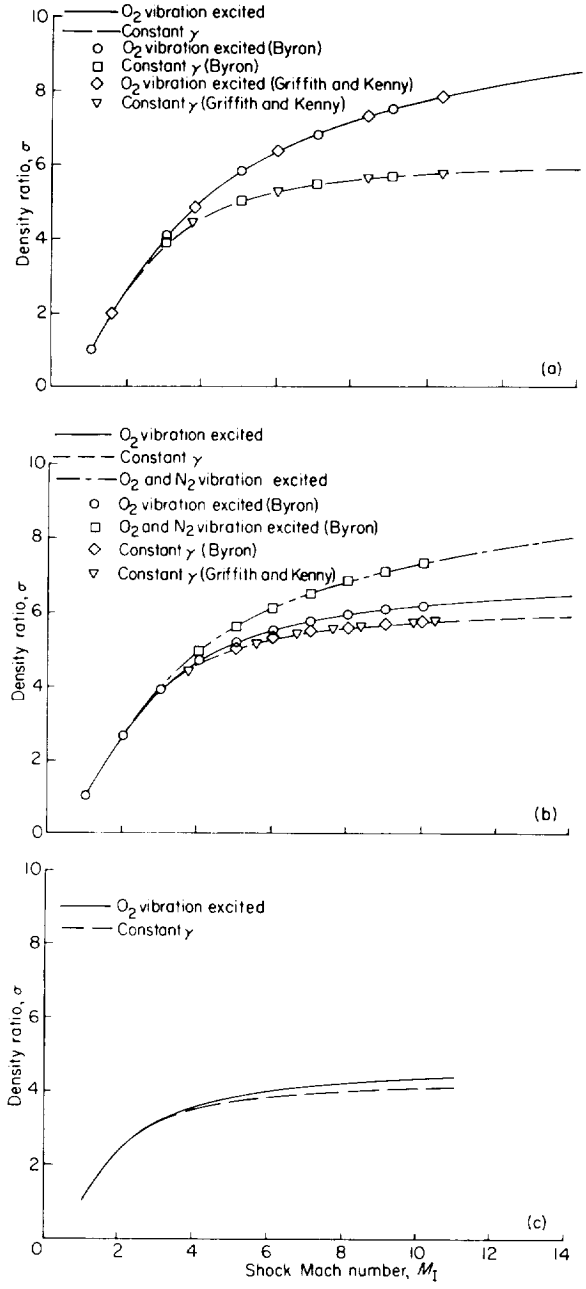

(a) Oxygen.
(b) Air.
(c) 10 percent O_2 in argon.

FIGURE 30.—Calculated values of density behind shock fronts. $\alpha = 0$.

72. These results are also shown in figures 29 and 30 for comparison with the results obtained herein. The curves shown in the figures are of three types. One is labeled "Constant γ" and is based on the assumption that only the translational and rotational degrees of freedom of the molecules are excited. A second type is labeled "O_2 vibration excited" and is based on the assumption that the vibrational degree of freedom of the oxygen molecule is excited in addition to the translational and rotational degrees. The third type applies only to air and is based on the assumption that vibration is fully excited for both oxygen and nitrogen. The above assumptions enter into the solution of equations (19) and (22) through the enthalpy function η in equation

(19). Vibrationally unexcited oxygen and nitrogen were both assumed to have a specific-heat ratio of $\gamma = 1.4$. The value $\gamma = 1.67$ was used for argon. For the cases in which vibrational excitation was assumed for oxygen or nitrogen the enthalpy data were taken from reference 73 for temperatures up to 5,000° K and from reference 74 for temperatures between 5,000° and 10,000° K. Excitation of the $a(^1\Delta_g)$ and $b(^1\Sigma_g^+)$ electronic states was found to have a negligible effect on the enthalpy for these temperatures. It was pointed out previously, however, that excitation of these states has an important effect on the distribution of the oxygen molecules over the vibrational levels of the initial electronic state.

For a given shock-tube test only one of the above assumptions corresponded to the actual conditions present behind the shock. In figures 31, 32, and 33 experimental and theoretical values of the light transmission are compared. The theoretical curves are based on the assumptions

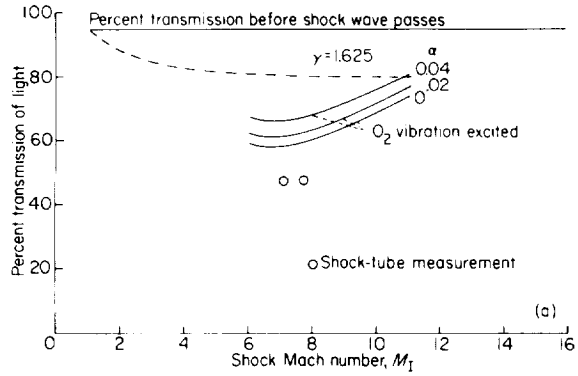

(a) $\lambda = 1{,}300$ angstrom units; $p_1 = 5$ millimeters.

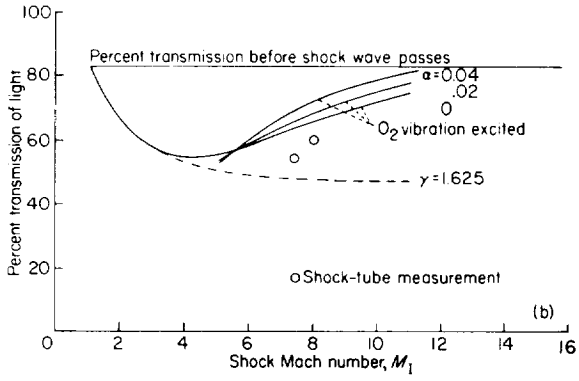

(b) $\lambda = 1{,}350$ angstrom units; $p_1 = 3$ millimeters.

FIGURE 31.—Calculated and observed percent transmission of light for oxygen-argon mixture.

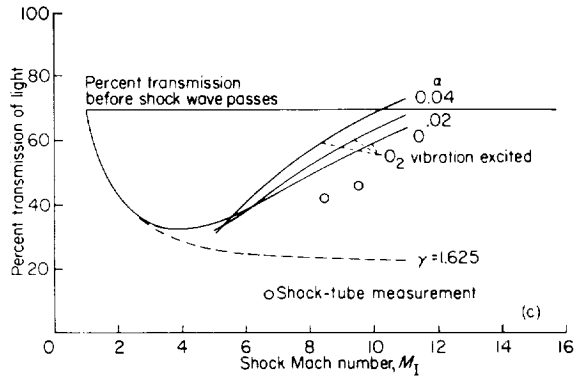

(c) $\lambda = 1{,}400$ angstrom units; $p_1 = 3$ millimeters.

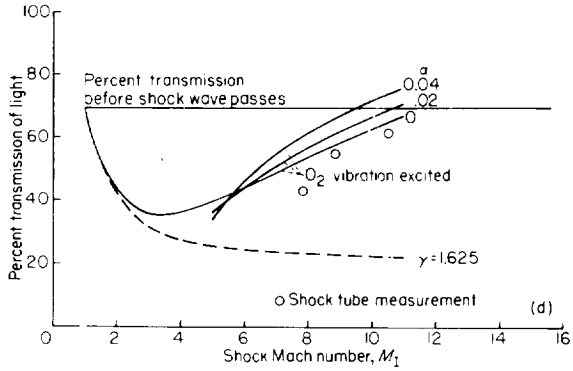

(d) $\lambda = 1{,}450$ angstrom units; $p_1 = 3$ millimeters.

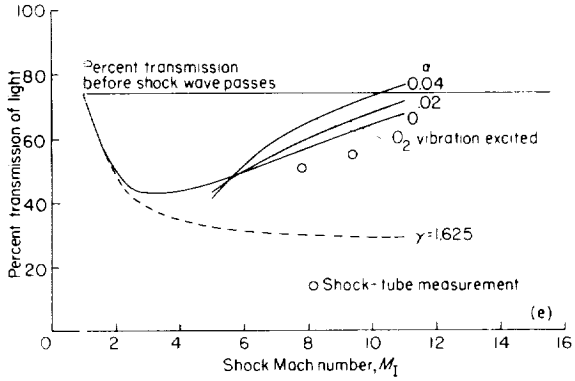

(e) $\lambda = 1{,}500$ angstrom units; $p_1 = 3$ millimeters.

FIGURE 31.—Continued.

mentioned and on the best estimate values of $\hat{k}$ which are listed in table I. Note that table I contains two sets of best estimate values. One of these corresponds to excitation of the $N(^3\Sigma_g^-)$ electronic state only and was used for the oxygen-argon curves. The other corresponds to excitation of the $a(^1\Delta_g)$ and $b(^1\Sigma_g^+)$ states as well and was used for the air and pure oxygen curves. Best agreement between theory and experiment

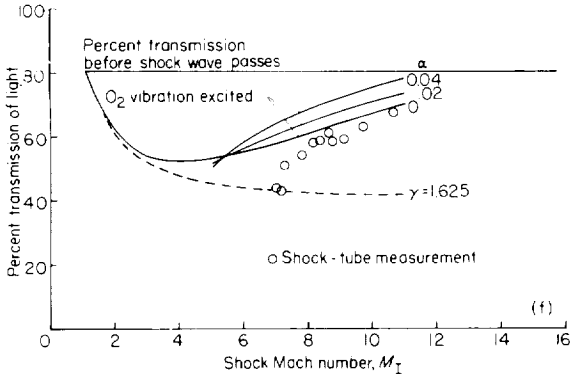

(f) λ=1,550 angstrom units; p_1=3 millimeters.

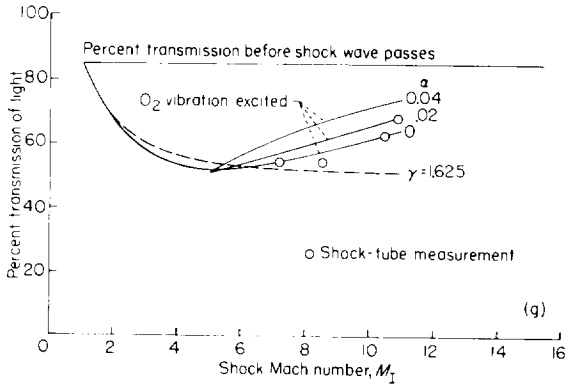

(g) λ=1,600 angstrom units; p_1=4 millimeters.

FIGURE 31.—Continued.

was obtained in this way. Examination of figures 31 and 32 shows that dissociation affected the magnitude of the measured light intensity jumps at the highest temperatures. In order to account for this the calculation of $\hat{k}_{II}$ from equation (14) was modified as shown in appendix D.

The remaining quantity to be evaluated was $\hat{\rho}_1$. From equation (18), $p_s=\rho_s RT_s$ and $p_1=\rho_1 RT_1$, where the subscript s refers to standard atmospheric conditions. Thus,

$$\hat{\rho}_1=g\rho_1/\rho_s=(p_1/p_s)(T_s/T_1)g \qquad (23)$$

Summary of data analysis.—The data analysis can be summarized as follows:

(1) $\hat{k}_{II}=(1/\sigma)\left[\hat{k}_I-\frac{\log_e(J_{II}/J_I)}{k_0^m\hat{\rho}_1 l}\right]$ (with modifications from appendix D) (eq. (14))

(2) T_{II} and σ were obtained from figures 29 and 30

(3) $\hat{k}_I$ was obtained from figure 19 (corrected IBM values)

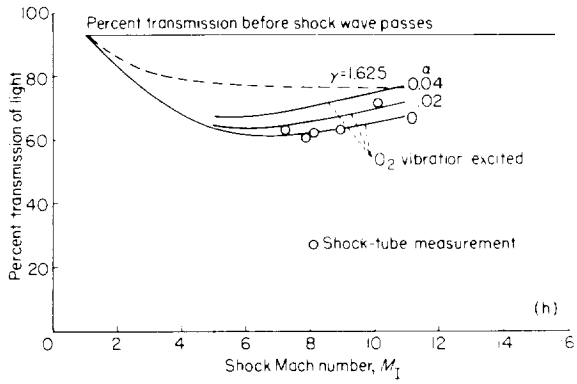

(h) λ=1,660 angstrom units; p_1=4 millimeters.

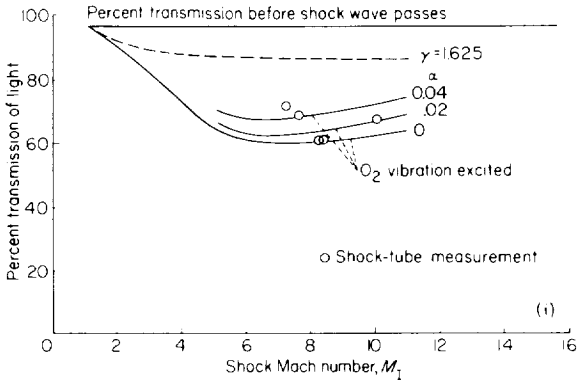

(i) λ=1,700 angstrom units; p_1=5 millimeters.

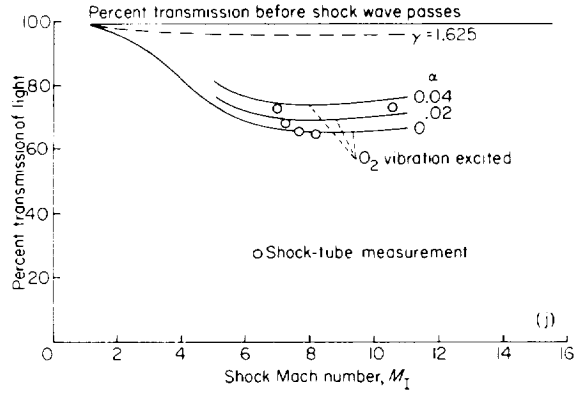

(j) λ=1,750 angstrom units; p_1=5 millimeters.

FIGURE 31.—Concluded.

(4) J_{II}/J_I was evaluated from the oscilloscope records

(5) $\hat{\rho}_1=(p_1/p_s)(T_s/T_1)g$ (eq. (23))

(6) The absorption path length l was always 2.54 centimeters

(7) λ, T_1, and p_1 were recorded at the time the data were taken

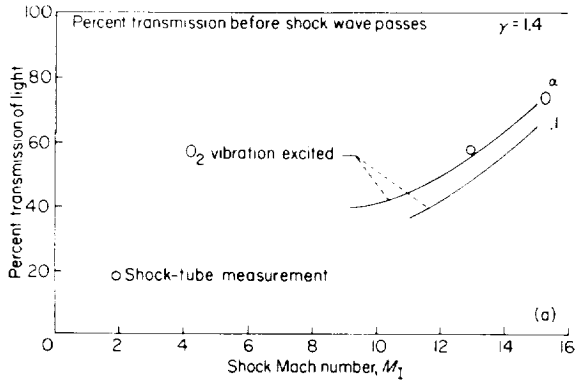

(a) $\lambda = 1{,}300$ angstrom units; $p_1 = 0.5$ millimeter.

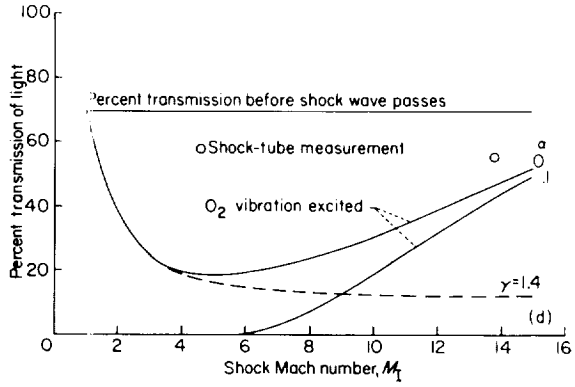

(d) $\lambda = 1{,}450$ angstrom units; $p_1 = 0.3$ millimeter.

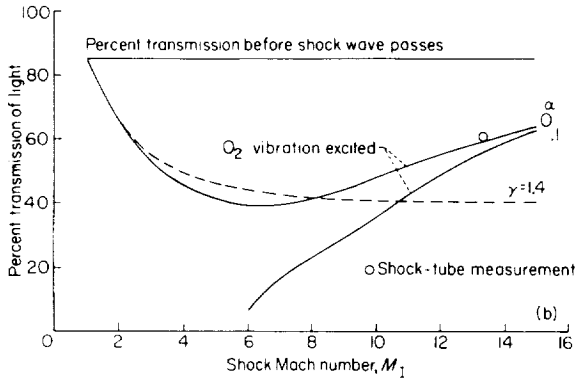

(b) $\lambda = 1{,}350$ angstrom units; $p_1 = 0.3$ millimeter.

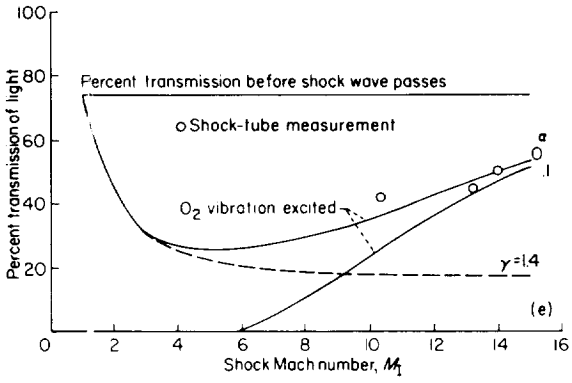

(e) $\lambda = 1{,}500$ angstrom units; $p_1 = 0.3$ millimeter.

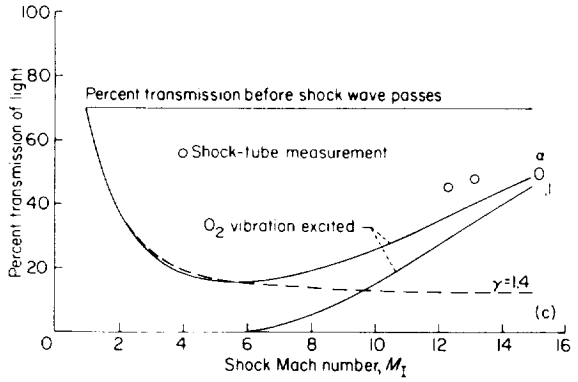

(c) $\lambda = 1{,}400$ angstrom units; $p_1 = 0.3$ millimeter.

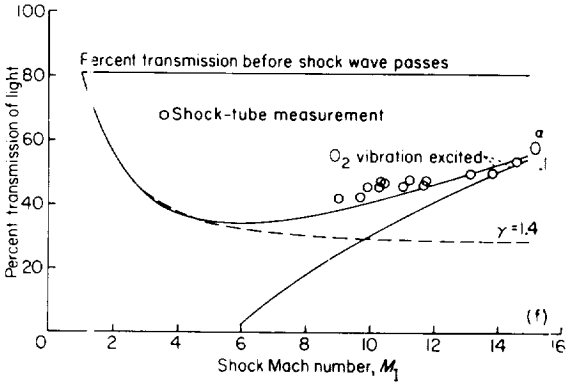

(f) $\lambda = 1{,}550$ angstrom units; $p_1 = 0.3$ millimeter.

FIGURE 32.—Calculated and observed percent transmission of light for oxygen.

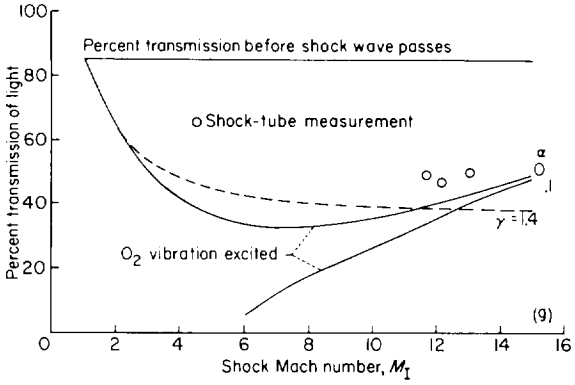

(g) λ =1,600 angstrom units; p_1=0.4 millimeter.

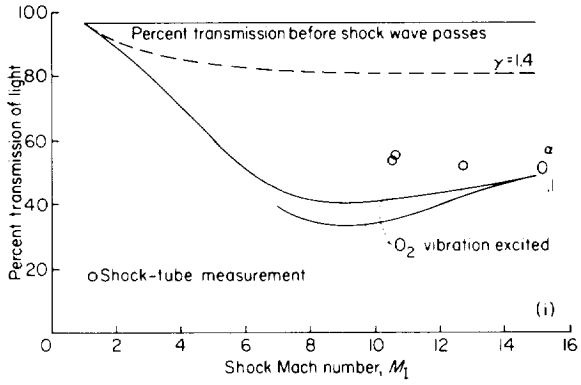

(i) λ=1,700 angstrom units; p_1=0.5 millimeter.

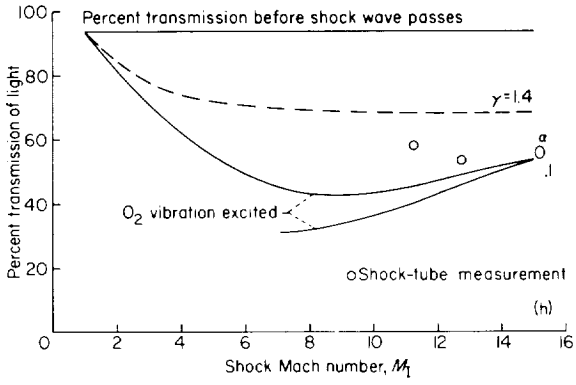

(h) λ=1,660 angstrom units; p_1 =0.4 millimeter.

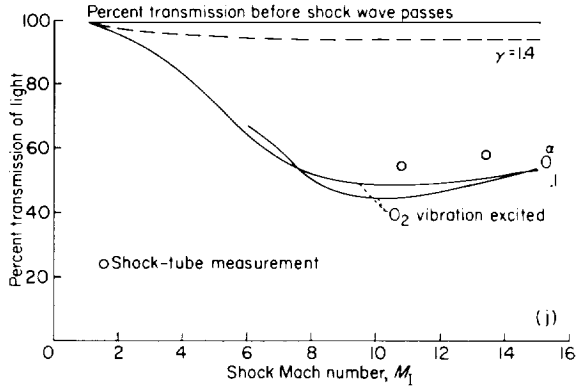

(j) λ=1,750 angstrom units; p_1=0.5 millimeter.

FIGURE 32.—Concluded.

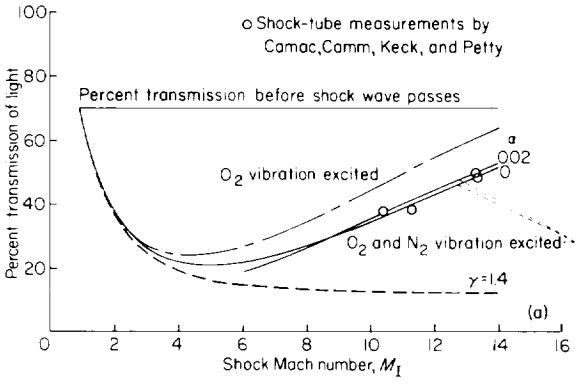

(a) λ=1,470 angstrom units; p_1=1 millimeter.

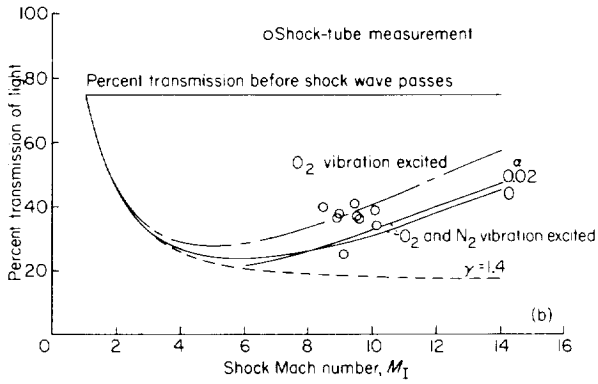

(b) λ=1,550 angstrom units; p_1 =2 millimeters.

FIGURE 33.—Calculated and observed percent transmission of light for air.

PRESENTATION OF EXPERIMENTALLY MEASURED ABSORPTION COEFFICIENTS

Cross plots of $\hat{k}$ as a function of temperature at 1,300, 1,350, . . . 1,750 angstrom units were prepared from the digital-computer results and are shown in figure 34. These serve as a comparison background for the experimental values of $\hat{k}$, that is, $\hat{k}_{II}$ from equation (14). For completeness, curves are shown both with and without the effect of the empirical correction for variable electronic transition probability and both with and without the assumption of complete equilibrium of initial electronic states. In addition, best-estimate curves are shown for wavelengths shorter than 1,375 angstrom units. For wavelengths longer than 1,375 angstrom units best-estimate curves are identical to corrected IBM curves.

DISCUSSION OF RESULTS

PRELIMINARY REMARKS

As was pointed out previously, both theoretical and experimental approaches were made to the problem of determining the effect of temperature on the absorption coefficient. The Franck-Condon principle which underlies the theoretical treatment is well established and has proved over the years to be capable of accurate prediction of transition probabilities when all the pertinent factors are known. From the outset the intention of the present investigation was to calculate the temperature dependence from the theoretical treatment and then to attempt to verify or to disprove the results by experimental measurement

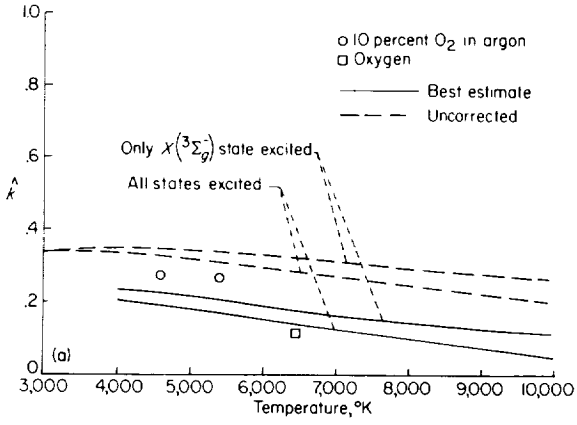

(a) $\lambda = 1{,}300$ angstrom units.

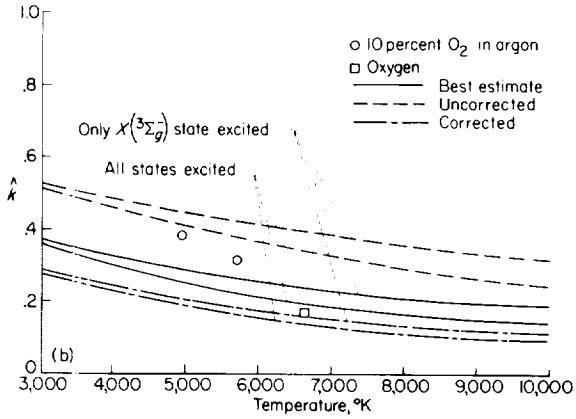

(b) $\lambda = 1{,}350$ angstrom units.

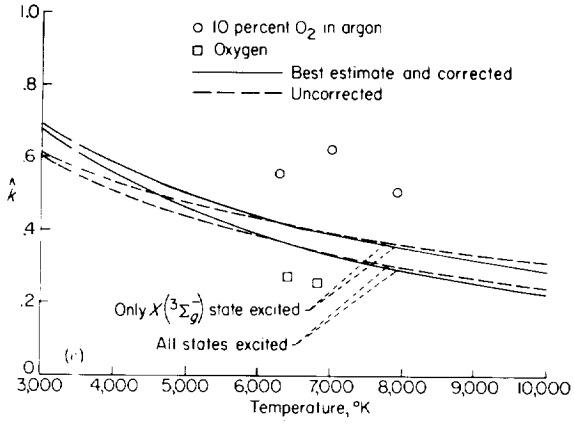

(c) $\lambda = 1{,}400$ angstrom units.

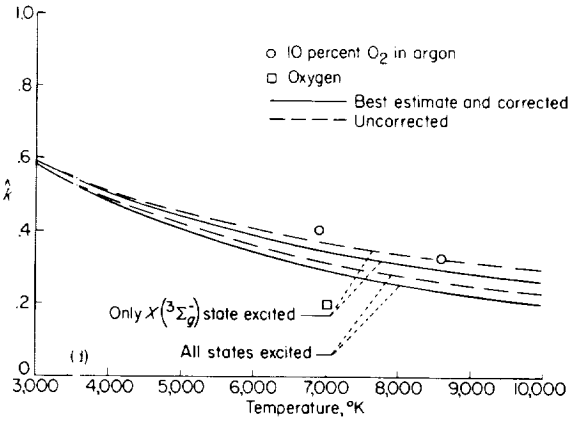

(d) $\lambda = 1{,}450$ angstrom units.

FIGURE 34.—Absorption coefficient of molecular oxygen as a function of temperature at selected wavelengths.

of the absorption in a shock tube. This program was carried out satisfactorily.

At most wavelengths and temperatures the agreement between theory and experiment is good enough to show that the theory is essentially

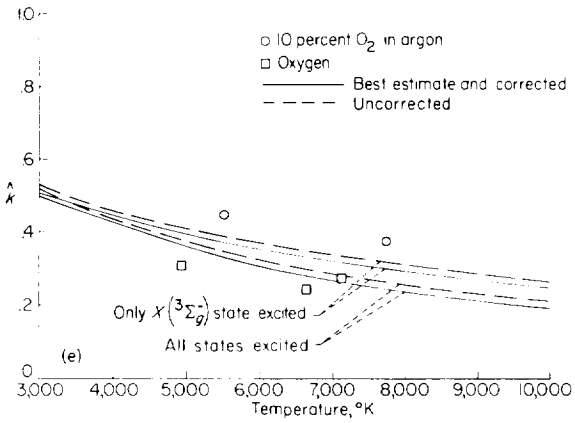

(e) λ—1,500 angstrom units.

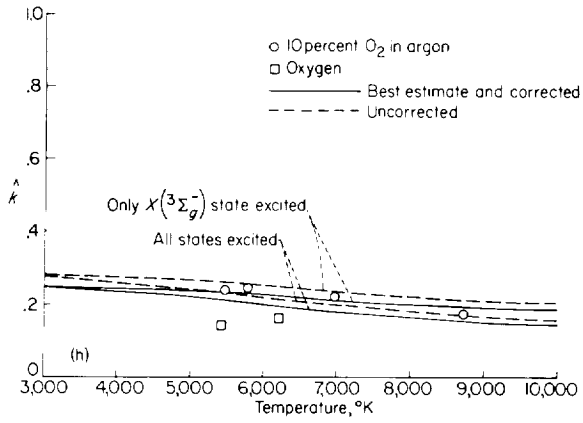

(h) λ 1,660 angstrom units.

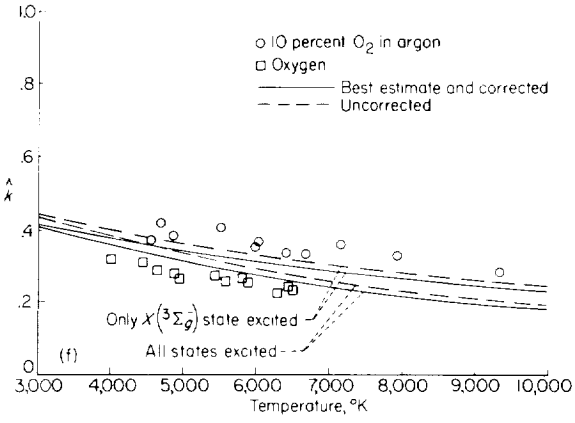

(f) λ 1,550 angstrom units.

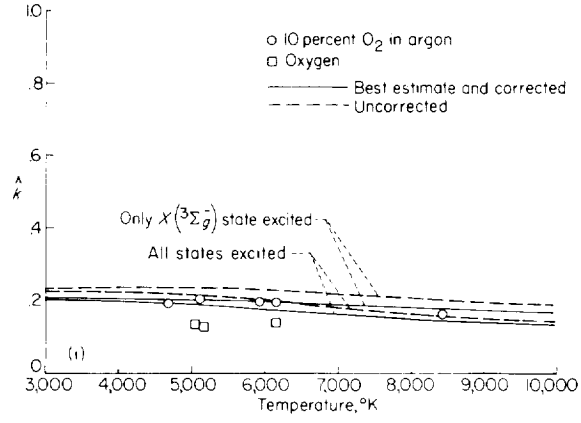

(i) λ 1,700 angstrom units.

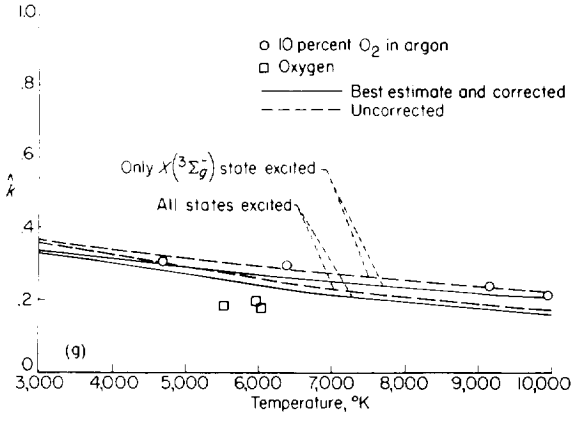

(g) λ=1,600 angstrom units.

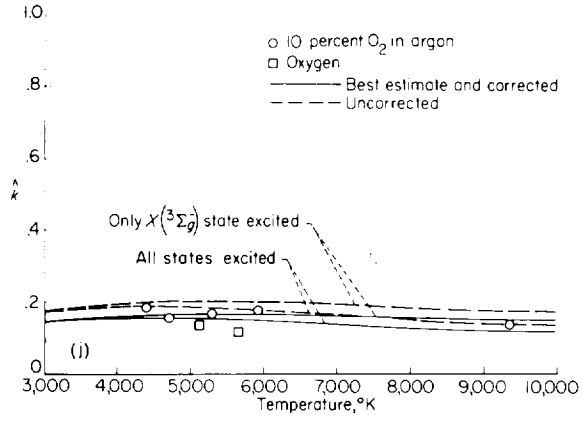

(j) λ=1,750 angstrom units.

FIGURE 34.—Concluded.

correct. Where disagreements exist plausible explanations are available. Because of experimental uncertainties and the possibility of systematic errors, the corrected IBM results were selected as the best available estimate of the absorption coefficient except in the areas where experiment showed definite disagreement with theory. Empirical curves based chiefly on the observed absorption were prepared for use in these areas.

COMPARISON OF THEORY AND EXPERIMENT AT ROOM TEMPERATURE

The three curves in figure 35(a) show the results of the three theoretical calculations at 300° K. Since the experimental results did not include any values at room temperature, the data of references 1 to 6, shown in figure 2, were replotted in figure 35(a) for comparison with the theory.

In figure 35(b) the reference data are compared with the IBM theoretical curves both with and without the empirical correction for variation of the electronic transition probability with internuclear distance. Note that the peak of the corrected curve rises higher than the value $k_0^m = 400$ cm^{-1}.

In figure 35(a) the wavelength at which maximum absorption occurs is 1,450 angstrom units for the IBM curve and is 1,455 angstrom units for the other two curves. Figure 35(b) shows that the corrected IBM curve has a very flat peak centered at about 1,430 angstrom units. The experimental peak lies somewhere between 1,400 and 1,475 angstrom units, and thus it is not possible to distinguish between the calculated peak values.

Theory and experiment agree well on the long-wavelength side of the curve (1,450 to 1,750 angstrom units). However, the scatter of the

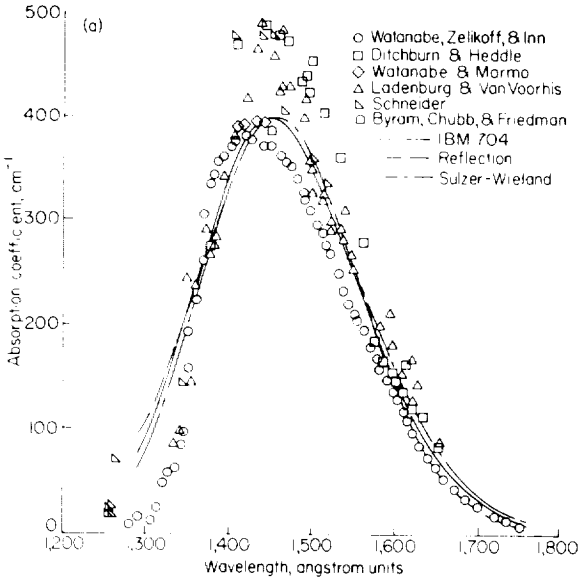

(a) Comparison of experimental data and data obtained from IBM 704, by reflection method, and by Sulzer-Wieland method.

FIGURE 35. Absorption coefficient of molecular oxygen, 300° K.

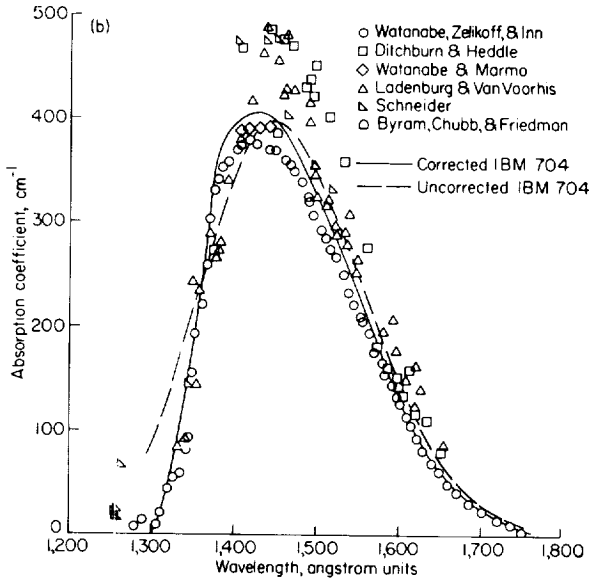

(b) Comparison of experimental data and corrected and uncorrected IBM 704 data.

FIGURE 35.—Concluded.

experimental points is too great to permit a choice to be made among the various theories. Except for the corrected IBM curve, theory and experiment do not agree on the short-wavelength side (1,250 to 1,450 angstrom units). Note that the absorption coefficients measured by three independent investigators (refs. 1, 4, and 5) show the rapid drop of the experimental points in this region. This is convincing evidence that the deviation from the theoretical curves in figure 35(a) is real. Little significance can be attached to the agreement in figure 35(b) between the corrected IBM curve and the data because the correction was designed to make the curve fit the room-temperature data.

Camac and Vaughan (ref. 9) measured the room-temperature absorption at 1,470 angstrom units. The exact value found was not given, but the value $k_0 = 307$ cm^{-1} was derived from the slope of the Beer's law plot shown in figure 7 of reference 9. This is smaller than other values reported in the literature, which range from 365 to 465 cm^{-1}. The best-estimate value of k_0 at 1,470 angstrom units and 300° K from the work reported here is $400(0.940) = 376$ cm^{-1}.

COMPARISON OF THEORY AND EXPERIMENT AT HIGH TEMPERATURE

The experimental results at high temperature are shown in figure 34. As was mentioned

previously, the comparison curves are cross plots of $\hat{k}$ against temperature and are based on both corrected and uncorrected IBM calculations. Alternate curves are included to illustrate the effect of the lack of complete excitation of the initial electronic states. Below 1,375 angstrom units the best-estimate curves are also shown because they are not identical to the corrected IBM results in this region.

In figure 36 the high-temperature absorption coefficients measured by Camac and Vaughan are compared with the best-estimate theoretical curves. As noted in the figure, the data points plotted are not exactly as given in reference 9. The quantity $69/\sigma$ was added to each point to compensate for the use of $k_0=307$ cm^{-1} for the room-temperature absorption coefficient instead of the value $k_0=376$ cm^{-1}.

Some of the shock-tube runs were not suitable for the determination of $\hat{k}$ because vibration was not in equilibrium behind the shock front. Generally such runs were not used although some exceptions were made for records on which only a short extrapolation back to the shock jump was required. All runs were plotted in figures 31, 32, and 33, however. The next few paragraphs explain how the plots in these figures were used to determine which runs should be excluded because of the lack of vibrational equilibrium

The description of data-analysis procedure given previously pointed out that the T_{II} and σ values appropriate for the calculation of $\hat{k}$ from equation (14) depend upon the state of vibrational excitation of the components of the gas mixture being tested. The comparison of observed light transmission to that expected on the basis of the two or three possible states of vibrational excitation is the most important single indication of the actual state of the gas but is sometimes ambiguous and misleading when unsupported by additional evidence.

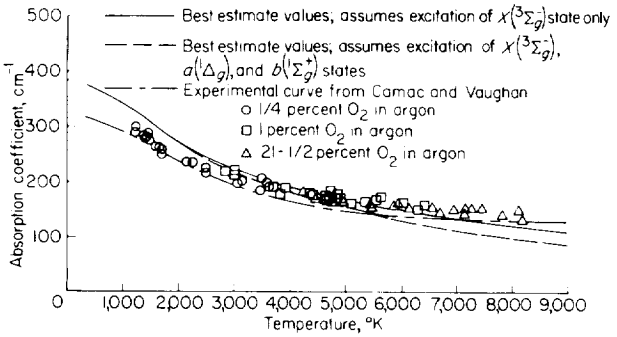

FIGURE 36.—Absorption coefficient of molecular oxygen as a function of temperature at 1,470 angstrom units. Data points are from Camac and Vaughan (ref. 9). The quantity $69/\sigma$ was added to each point because $k_0=376$ cm^{-1} is believed to be more nearly correct than $k_0=307$ cm^{-1}, which is approximately the value they used.

The data on air shown in figure 33 are a good example of this. The four data points from the literature plotted in figure 33(a) seem to show that oxygen and nitrogen vibration are both fully excited for all four points but examination of the oscilloscope records revealed relaxation regions behind the fronts of the two slowest shock waves which must be interpreted as nitrogen vibrational relaxation because of the direction of the adjustment (ref. 39, p. 9). This makes the slight upswing of the low-speed points toward the "O_2 vibration excited" curve appear significant. This conclusion is supported by the measured points in figure 33(b). The runs shown were obtained at $M_{\mathrm{I}}=10.1$ or below and, as expected, most of them are clustered close to the "O_2 vibration excited" curve. The nitrogen vibrational adjustment was visible on all these records. No values for $\hat{k}$ were obtained from the air records because the state of the gas behind the shock front was not well defined.

Figure 31(f) shows that between $M_{\mathrm{I}}=7$ and $M_{\mathrm{I}}=8$ in oxygen-argon mixtures the points turned toward the constant γ curve, indicating that oxygen vibration was not in equilibrium. This conclusion is substantiated by the observation that the vibrational adjustment was clearly visible on the corresponding records.

Vibrational relaxation was not observed on any of the records taken in pure oxygen. Also the data points in figure 32(f) do not turn toward the constant γ curve as they did in figure 31(f). These two statements both indicate that vibrational relaxation of pure oxygen was too fast to observe on the records taken. The previously mentioned inability of the shock detector stations to function properly below about 4,000° K prevented the determination of the region where the oxygen points bend toward the constant γ curve.

The net effect of the above observations relating to vibrational adjustments was to cause most of the oxygen-argon records below $M_{\mathrm{I}}=8$ to be rejected. All the air runs were rejected, but it was

not necessary to reject any of the oxygen runs, although a limitation no doubt exists.

Certain general characteristics of the observed data can be brought out more clearly if they are noted before becoming involved in the discussions of the individual mixtures. An examination of figure 34 reveals that:

(1) The values of $\hat{k}$ obtained from the oxygen-argon mixtures are always larger than those obtained from pure oxygen. This follows a definite pattern at all wavelengths and temperatures. The data from either gas are internally consistent but disagree when compared with each other.

(2) The excess of $\hat{k}$ varies with wavelength and is generally larger at the shorter wavelengths.

(3) The excess of $\hat{k}$ varies little, if any, with temperature.

(4) The corrected IBM curve, which at the longer wavelengths stays quite close to the uncorrected IBM curve, falls far below it at wavelengths shorter than 1,375 angstrom units. Both the oxygen and the oxygen-argon points show a tendency to follow this trend but do not go as far. This effect leads to the conclusion that the correction is needed but also tends to confirm the suspicion stated previously that the empirical correction is inaccurate below 1,375 angstrom units.

The following observations about the oxygen-argon results are based on an examination of figure 34 and are restricted to wavelengths longer than 1,375 angstrom units:

(1) The data points agree best with the curves for which only the ground electronic state $X(^3\Sigma_g^-)$ is excited.

(2) The scatter of the points is too large to distinguish between the corrected and uncorrected IBM curves.

(3) In the range 1,400 to 1,550 angstrom units the data points fall higher than any of the theoretical curves. This could indicate the presence of extra absorption due to the presence of argon. However, the measurements of Camac and Vaughan at 1,470 angstrom units (fig. 36) show no indication of any extra absorption. Also the wavelengths used were too long to excite even the lowest excited state of argon (λ=1,048 angstrom units). In spite of this absorption records were taken in pure argon (less than 0.1 percent O_2 by analysis) at 1,500, 1,550, 1,660, and 1,700 angstrom units to check for the presence of absorption jumps. None were observed at 1,660 and 1,700 angstrom units, but they were present at 1,500 and 1,550 angstrom units. Figure 37 shows the record obtained at 1,550 angstrom units. The jump corresponds to the presence of about 4 percent O_2, but chemical analysis accurate to ± 0.1 percent showed no trace of it.

The following observations about the oxygen results are based on an examination of figure 34 and are restricted to wavelengths larger than 1,375 angstrom units:

(1) The points agree best with the curves for which the electronic states are in equilibrium.

(2) The scatter of the points is too large to distinguish between the corrected and uncorrected IBM curves.

(3) There is no indication of extra absorption. This tends to reinforce the suspicion that argon was responsible for the previously mentioned extra absorption.

(4) With few exceptions the points fall low as compared with the theoretical curves although they do show the expected temperature dependence. Emitted light from the shocked oxygen could explain the discrepancy, but, as was mentioned in the section in which the experimental measurements are described, no evidence of emitted light was observed.

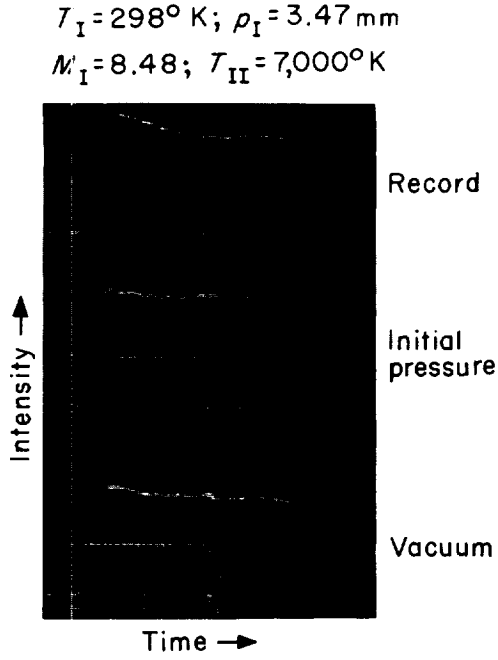

FIGURE 37.—Record of absorption jump in pure argon. λ=1,550 angstrom units. Time base on record is 10 microseconds per centimeter.

BEST ESTIMATE OF $\hat{k}$ AT HIGH TEMPERATURE

The best-estimate values of $\hat{k}$ at high temperature were based on the following considerations:

(1) Above 1,375 angstrom units the corrected IBM results were considered to be the best estimate of the high-temperature absorption coefficient of oxygen.

(2) Below 1,375 angstrom units empirically determined curves corresponding to $\hat{k}$ values intermediate between the corrected and uncorrected IBM curves were considered to be the best estimate. These curves were drawn roughly parallel to the corrected IBM curves and bear approximately the same relationship to the measured data as the curves at wavelengths greater than 1,375 angstrom units.

Values of $\hat{k}$ as functions of temperature and wavelength are listed in table I. Best-estimate, corrected, and uncorrected values are given both for complete electronic excitation and for $X(^3\Sigma_g^-)$ state excitation only.

CONCLUSIONS

A theoretical and experimental investigation of the absorption coefficient of molecular oxygen at high temperature led to the following conclusions:

1. In accordance with the customary behavior of absorption continua in diatomic gases, the peak value of the absorption coefficient decreases with temperature.

2. The breadth of the absorption peak increases with temperature so that at wavelengths not too close to the peak the absorption coefficient increases with temperature. The broadening also extends the continuum to longer wavelengths than those for which absorption is observed at room temperature.

3. For wavelengths longer than 1,375 angstrom units, the temperature dependence and wavelength distribution are best given by the results of a digital-computer calculation which has been corrected for variation of the electronic transition probability with internuclear distance.

4. For wavelengths shorter than 1,375 angstrom units, the best values of the absorption coefficient are given by empirical curves with shapes determined by theory and magnitudes determined by experiment.

5. For shock waves in pure oxygen the observed values of the absorption coefficient indicate that electronic excitation of oxygen is complete immediately behind the shock front.

6. For shock waves in a mixture of 10 percent oxygen in argon the observed values of the absorption coefficient indicate that the electronic states of oxygen are unexcited immediately behind the shock front.

LANGLEY RESEARCH CENTER,
NATIONAL AERONAUTICS AND SPACE ADMINISTRATION,
LANGLEY FIELD, VA., *September 14, 1960.*

APPENDIX A

PROCEDURE USED IN CALCULATING THE POTENTIAL CURVE FOR $B(^3\Sigma_u^-)$ STATE

Equation (8) shows that k/E^* is proportional to $\tilde{a}^{-1/3}\phi_{v'}^2$. Since k and E^* are known as functions of λ from room-temperature data and ϕ_0 was calculated as a function of r from the Morse potential, a relation between λ and r_s was found by comparing properly normalized plots of k/E^* against $\tilde{\nu}$ and $\tilde{a}^{-1/3}\phi_0^2$ against r_s. The following procedure describes how this was done:

(1) Two plots of $k\lambda/(k\lambda)_{max}$ against $\tilde{\nu}$ were prepared. One was based on the data of Watanabe, Zelikoff, and Inn (ref. 1), and the other, on the experimentally determined absorption curve given by Ditchburn and Heddle (ref. 2). The curves found in this way are shown in figure 38.

(2) A plot of $C_3\tilde{a}^{-1/3}\phi_0^2$ against r_s is shown in figure 39. A value of C_3 was chosen to make the maximum ordinate unity. As shown in appendix B, the use of a delta function for the upper-state eigenfunction requires the integral in equation (3) to vanish except for $r=r_s$. Thus, r_s was used in figure 39 rather than r.

(3) Corresponding λ, r_s pairs were tabulated by finding $\tilde{\nu}$ and r_s for $k\lambda/(k\lambda)_{max}=C_3\tilde{a}^{-1/3}\phi_0^2$. A separate tabulation was prepared for each of the experimental absorption curves of figure 38.

(4) By adding to $\tilde{\nu}$ the energy of the initial state as calculated from the Morse potential, the points shown in figures 12 and 13 were found. The B state potential curve shown in figure 13 was determined by fairing a curve through these points and through the Rydberg-Klein-Rees points.

Note that it is assumed in this procedure that $k_0(\lambda)$ can be correctly calculated from a knowledge of the initial-state wave functions and the upper-state potential curve by using the reflection method. Coolidge, James, and Present (ref. 19, p. 203) point out that this assumption is not strictly correct although it is a good approximation for $v''=0$ (fig. 6, p. 204, of ref. 19). The most serious error caused by using the reflection method is a shift of the peak of the distribution curve toward longer wavelengths. This shift is caused by the fact that maximum absorption occurs when the relative orientation of the initial and final wave functions is such that the overlap integral $\int_0^\infty \phi_{v''}\psi dr$ is maximized rather than when the turning point of the upper-state wave function occurs at the same value of internuclear distance as the peak of the lower-state wave function.

Upon completion of the digital-computer calculations based on the potential found as just described a plot of $C_4\tilde{a}^{-1/3}\left(\int_0^\infty \phi_0\psi dr\right)^2$ against r_s was added to figure 39. As before, the constant was chosen to make the maximum ordinate unity. The good agreement with the plot of $C_3\tilde{a}^{-1/3}\phi_0^2$

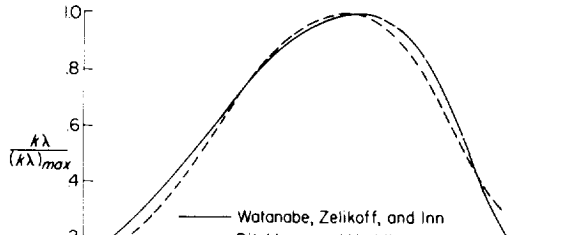

FIGURE 38.—Ratio $k\lambda/(k\lambda)_{max}$ as a function of $\tilde{\nu}$.

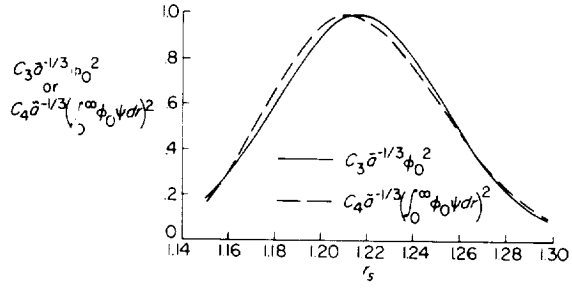

FIGURE 39.—The expressions $C_3\tilde{a}^{-1/3}\phi_0^2$ and $C_4\tilde{a}^{-1/3}\left(\int_0^\infty \phi_0\psi dr\right)^2$ as functions of r_s.

verifies that the reflection method is a good approximation for $v''=0$.

The two curves of figure 39 were used together with the Watanabe, Zelikoff, and Inn curve of figure 38 to plot the points shown in figure 14. The curve of E^* plotted against r_s shown in figure 14 was derived from the B state potential used in all the calculations and it is satisfying to observe that the set of data points based on the digital-computer calculations agrees with this curve better than do the reflection data points, even though the difference is in most cases quite small.

APPENDIX B

DERIVATION OF EQUATION (8)

As was stated in equation (3), the absorption coefficient $k_{v''}(\lambda)$ is proportional to certain factors. The most important of these is the vibrational overlap integral $\int_0^\infty \phi_{v''}\psi dr$. Replacing the ψ function by a delta function located at the turning point permits the integral to be evaluated, that is, $\int_0^\infty \phi_{v''}\psi dr=\phi_{v''}(r_s)$, where r_s is the value of r at the turning point of the B state.

Normalized Morse functions were used for obtaining $\phi_{v''}$. It was not necessary to normalize the delta functions used to replace ψ because the normalization factor F for the ψ function appears explicitly in equation (3). The derivation of the factor F is given in appendix C. Substitution of $F=241.89\tilde{E}^{1/4}\tilde{a}^{-1/6}$ and $\int_0^\infty \phi_{v''}\psi dr=\phi_{v''}(r_s)$ into equation (3) gives the following result (eq. (8)):

$$\hat{k}_{v''}(\lambda)=\text{Constant}\ \tilde{a}^{-1/3}E^*\phi_{v''}{}^2$$

where $(241.89)^2$ has been absorbed into the proportionality constant and the whole equation has been divided by k_0^m.

APPENDIX C

DERIVATION OF NORMALIZATION FACTOR FOR ψ WAVE FUNCTION

The fact that Hankel functions satisfy the Schrödinger equation when V is linear has already been mentioned. The normalization factor was derived by suitably comparing the Hankel function solution for ψ, which is a good approximation near the turning point, to the Wentzel-Kramers-Brillouin (WKB) solution (discussed in ref. 34, p. 178), which is a good approximation everywhere except near the turning point. The reasoning is as follows:

(1) Except for a constant factor the asymptotic Hankel amplitude is identical to the WKB amplitude for the same potential. Let the potential used for the WKB function depart from a straight line at some point distant from the turning point and let it approach the dissociation energy of the B state as r approaches infinity. Normalize the WKB amplitude to unity at infinity.

(2) The desired normalization factor is the factor required to make the Hankel amplitude coincide with the normalized WKB amplitude in the region where both are derived from a straight-line potential.

(3) The value of the Hankel function at the turning point is given as 1.074 in the tables used (ref. 75) and this value was always used for the value of ψ at the starting point for the integration of equation (10).

(4) The value of ψ at the turning point of a Hankel function is (ref. 34, p. 183)

$$\psi(r_s)=\frac{A(2/3)^{1/2}(3)^{-1/3}\left(\frac{8\pi^2\mu\tilde{a}}{h^2}\right)^{-1/6}}{\Gamma(2/3)}$$

where $\tilde{a}$ is the slope of the B state potential curve at the turning point.

(5) Setting $\psi(r_s)$ equal to 1.074 gives

$$A=2.09226\times10^5\tilde{a}^{1/6}$$

(6) The asymptotic Hankel amplitude is

$$f_H=1.7318A(\pi b/2)^{-1/2}=\frac{(1/2.4189)\tilde{a}^{1/6}}{\tilde{a}^{1/4}(r-r_s)^{1/4}}$$

where

$$b=\{(2\pi/h)[2\mu(E-V')]^{1/2}\}_{r\to r_s}$$
$$=(2\pi/h)[2\times10^{-8}\mu\tilde{a}(r-r_s)]^{1/2}$$

(See ref. 34, eqs. (28.16) and (28.17).) The Hankel function used is $u^+ + u^-$ in Schiff's notation. The factor 1.7318 is the sum of $\exp(-\pi i/6)$ and $\exp(-5\pi i/6)$.

(7) The corresponding normalized WKB amplitude is

$$f_{WKB}=\frac{1.7318A(\pi b/2)^{-1/2}}{1.7318A(\pi b_\infty/2)^{-1/2}}=(b/b_\infty)^{-1/2}$$

where

$$b_\infty=\{(2\pi/h)[2\mu(E-V')]^{1/2}\}_{r\to\infty}=(2\pi/h)(2\mu\tilde{E})^{1/2}$$

$$f_{WKB}=(b/b_\infty)^{-1/2}=\frac{10^2\tilde{E}^{1/4}}{\tilde{a}^{1/4}(r-r_s)^{1/4}}$$

(8) The desired normalization factor is

$$F=f_{WKB}/f_H=241.89\tilde{E}^{1/4}\tilde{a}^{-1/6}$$

(9) Substitution of F into equation (3) gives

$$k_{v''}(\lambda)=C\tilde{a}^{-1/3}F^*\left(\int_0^\infty\phi_{v''}\psi dr\right)^2$$

where $(241.89)^2$ has been absorbed into the constant C.

APPENDIX D

MODIFICATION OF CALCULATION OF $\hat{k}_{II}$ TO ACCOUNT FOR PRESENCE OF DISSOCIATION BEHIND THE SHOCK FRONTS

The calculation of $\hat{k}_{II}$ was modified as follows to account for the presence of dissociation behind the shock front:

(1) Plots of T_{II} and σ similar to those shown in figures 29 and 30 were prepared for partially dissociated mixtures. Oxygen vibration was assumed to be fully excited.

(2) The dissociation rate of oxygen was combined with the values of T_{II}, σ, and degree-of-dissociation relations obtained from the figures just mentioned to calculate the state of the gas as a function of distance from the shock front. The rates used were obtained from a separate investigation in which the same records used for the determination of the absorption coefficient were also analyzed for the dissociation rate of oxygen.

(3) While the shock wave was passing through the light beam the trace on the oscilloscope rose too rapidly to be recorded. Therefore, the observed jump in absorption on the record corresponded to the instant the shock wave left the light beam.

(4) Since the gas behind the shock front was flowing in the direction in which the shock wave was moving and at nearly the same speed, the gas within the 1-millimeter thickness of the light beam was made up not only of the gas originally there but also of all the gas which was originally in a considerable length of the shock tube preceding the test section. The ratio of these lengths was closely related to, but not quite proportional to, the compression ratio across the shock front.

(5) The 1-millimeter distance immediately behind the shock front was divided into several zones of unequal width. Zone width was determined so that an equal amount of dissociation occurred in each zone.

(6) Best-estimate values of $\hat{k}$ and appropriate values of T_{II}, σ, and degree of dissociation were used to compute the light transmission in each zone and a weighted average of the calculated light transmission through the shock-tube window was obtained by using the zone widths as weighting factors.

(7) The weighted average light transmission was compared with transmission calculated for gradually increasing dissociation on the assumption of uniform gas properties in the volume defined by the beam. The values of T_{II}, σ, and degree of dissociation for the uniform sample which gave the same transmission as the weighted average were used for the calculation of $\hat{k}_{II}$ in equation (14).

REFERENCES

1. Watanabe, K., Zelikoff, Murray, and Inn, Edward C. Y.: Absorption Coefficients of Several Atmospheric Gases. Geophys. Res. Papers No. 21 (AFCRC Tech. Rep. No. 53-23), Air Force Cambridge Res. Center, June 1953.
2. Ditchburn, R. W., and Heddle, D. W. O.: Absorption Cross-Sections in the Vacuum Ultra-Violet. I. Continuous Absorption of Oxygen (1800 to 1300 Å). Proc. Roy. Soc. (London), ser. A, vol. 220, no. 1140, Oct. 22, 1953, pp. 61–70.
3. Watanabe, K., and Marmo, F. F.: Photoionization and Total Absorption Cross Section of Gases. II. O_2 and N_2 in the Region 850 1500 A. Jour. Chem. Phys., vol. 25, no. 5, Nov. 1956, pp. 965 971.
4. Ladenburg, R., and Van Voorhis, C. C.: The Continuous Absorption of Oxygen Between 1750 and 1300A and Its Bearing Upon the Dispersion. Phys. Rev., vol. 43, no. 5, Second ser., Mar. 1, 1933, pp. 315–321.
5. Schneider, Edwin G.: An Estimate of the Absorption of Air in the Extreme Ultraviolet. Jour. Optical Soc. of America, vol. 30, no. 3, Mar. 1940, pp. 128–132.
6. Byram, E. T., Chubb, T. A., and Friedman, H.: Dissociation of Oxygen in the Upper Atmosphere. Phys. Rev., vol. 98, no. 6, Second ser., June 15, 1955, pp. 1594–1597.
7. Sulzer, P., and Wieland, K.: Intensitätsverteilung eines kontinuierlichen Absorptionsspektrums in Abhängigkeit von Temperatur und Wellenzahl. Helvetica Physica Acta, Bd. 25, Heft 6, 1952, pp. 653–676.
8. Stueckelberg, E. C. G.: Theory of Continuous Absorption of Oxygen at 1450A. Phys. Rev., vol. 42, no. 4, Second ser., Nov. 15, 1932, pp. 518–524.
9. Camac, M., and Vaughan, A.: Oxygen Vibration and Dissociation Rates in Oxygen-Argon Mixtures. Res. Rep. 84 (AFBMD-TR-60-22), Avco-Everett Res. Lab., Dec. 1959.
10. Gibson, G. E., Rice, O. K., and Bayliss, N. S.: Variation With Temperature of the Continuous Absorption Spectrum of Diatomic Molecules: Part II. Theoretical. Phys. Rev., vol. 44, no. 3, Second ser., Aug. 1, 1933, pp. 193–200.
11. Gibson, G. E., and Bayliss, Noel S.: Variation With Temperature of the Continuous Absorption Spectrum of Diatomic Molecules: Part I. Experimental, The Absorption Spectrum of Chlorine. Phys. Rev., vol. 44, no. 3, Second ser., Aug. 1, 1933, pp. 188–192.
12. Acton, A. P., Aickin, R. G., and Bayliss, N. S.: The Continuous Absorption Spectrum of Bromine: A New Interpretation. Jour. Chem. Phys., vol. 4, no. 8, Aug. 1936, pp. 474–479.
13. Britton, Doyle, Davidson, Norman, and Schott, Garry: Shock Waves in Chemical Kinetics—The Rate of Dissociation of Molecular Iodine. Discussions Faraday Soc., no. 17, 1954, pp. 58–68.
14. Britton, Doyle, Davidson, Norman, Gehman, William, and Schott, Garry: Shock Waves in Chemical Kinetics: Further Studies on the Rate of Dissociation of Molecular Iodine. Jour. Chem. Phys., vol. 25, no. 5, Nov. 1956, pp. 804–809.
15. Britton, Doyle, and Davidson, Norman: Shock Waves in Chemical Kinetics. Rate of Dissociation of Molecular Bromine. Jour. Chem. Phys., vol. 25, no. 5, Nov. 1956, pp. 810–813.
16. Palmer, H. B., and Hornig, D. F.: Rate of Dissociation of Bromine in Shock Waves. Jour. Chem. Phys., vol. 26, no. 1, Jan. 1957, pp. 98–105.
17. Herzberg, Gerhard: Molecular Spectra and Molecular Structure. I. Spectra of Diatomic Molecules. Second ed., D. Van Nostrand Co., Inc., c.1950.
18. Brix, P., and Herzberg, G.: Fine Structure of the Schumann-Runge Bands Near the Convergence Limit and the Dissociation Energy of the Oxygen Molecule. Canadian Jour. Phys., vol. 32, no. 2, Feb. 1954, pp. 110–135.
19. Coolidge, Albert Sprague, James, Hubert M., and Present, Richard D.: A Study of the Franck-Condon Principle. Jour. Chem. Phys., vol. 4, no. 3, Mar. 1936, pp. 193–211.
20. Nicholls, R. W., and Jarmain, W. R.: r-Centroids: Average Internuclear Separations Associated With Molecular Bands. Proc. Physical Soc. (London), vol. 69, pt. 3, no. 435A, Mar. 1, 1956, pp. 253–264.
21. Nicholls, R. W.: The Interpretation of Intensity Distributions in the CN Violet, C_2 Swan, OH Violet and O_2 Schumann-Runge Band Systems by Use of Their r-Centroids and Franck-Condon Factors. Proc. Physical Soc. (London), vol. 69, pt. 10, no. 442A, Oct. 1, 1956, pp. 741–753.
22. Morse, Philip M.: Diatomic Molecules According to the Wave Mechanics. II. Vibrational Levels. Phys. Rev., vol. 34, no. 1, Second ser., July 1, 1929, pp. 57–64.
23. Wu, Ta-You: The Vibrational Overlap Integral and the Intensities in Band Systems of Diatomic Molecules. Proc. Physical Soc. (London), vol. 65, pt. 12, no. 396A, Dec. 1, 1952, pp. 965–972.
24. Dunham, J. L.: Intensities in the Harmonic Band of Hydrogen Chloride. Phys. Rev., vol. 34, no. 3, Second ser., Aug. 1, 1929, pp. 438–452.
25. Dunham, J. L.: The Energy Levels of a Rotating Vibrator. Phys. Rev., vol. 41, no. 6, Second ser., Sept. 15, 1932, pp. 721–731.
26. Hulburt, Hugh M., and Hirschfelder, Joseph O.: Potential Energy Functions for Diatomic Molecules. Jour. Chem. Phys., vol. 9, no. 1, Jan. 1941, pp. 61–68.
27. Rees, A. L. G.: The Calculation of Potential-Energy Curves From Band-Spectroscopic Data. Proc. Physical Soc. (London), vol. 59, pt. 6, no. 336, Nov. 1, 1947, pp. 998–1008.

28. Vanderslice, Joseph T., Mason, Edward A., and Maisch, William G.: Interactions Between Ground State Oxygen Atoms and Molecules: O–O and O_2–O_2. Jour. Chem. Phys., vol. 32, no. 2, Feb. 1960, pp. 515–524.
29. Coolidge, Albert Sprague, James, Hubert M., and Vernon, E. L.: On the Determination of Molecular Potential Curves From Spectroscopic Data. Phys. Rev., vol. 54, no. 9, Second ser., Nov. 1, 1938, pp. 726–738.
30. Fraser, P. A., Jarmain, W. R., and Nicholls, R. W.: Vibrational Transition Probabilities of Diatomic Molecules; Collected Results II, N_2^+, CN, C_2, O_2, TiO. The Astrophysical Jour., vol. 119, no. 1, Jan. 1954, pp. 286–290.
31. Treanor, Charles E., and Wurster, Walter H.: Measured Transition Probabilities for the Schumann-Runge System of Oxygen. Jour. Chem. Phys., vol. 32, no. 3, Mar. 1960, pp. 758–766.
32. Golden, Joseph A., and Myerson, Albert L.: Recombination of Atomic Oxygen Observed by Means of the Flash Spectroscopy of Molecular Oxygen in the Vacuum Ultraviolet. Jour. Chem. Phys. (Letters to the Editor), vol. 28, no. 5, May 1958, pp. 978–979.
33. Margenau, Henry, and Murphy, George Moseley: The Mathematics of Physics and Chemistry. D. Van Nostrand Co., Inc., 1943.
34. Schiff, Leonard I.: Quantum Mechanics. McGraw-Hill Book Co., Inc., 1949.
35. Flory, Paul J.: Predissociation of the Oxygen Molecule. Jour. Chem. Phys., vol. 4, no. 1, Jan. 1936, pp. 23–27.
36. Volman, David H.: Photochemical Evidence Relative to the Excited States of Oxygen. Jour. Chem. Phys., vol. 24, no. 1, Jan. 1956, pp. 122–124.
37. Wilkinson, P. G., and Mulliken, R. S.: Dissociation Processes in Oxygen Above 1750 A. The Astrophysical Jour., vol. 125, no. 2, Mar. 1957, pp. 594–600.
38. Glick, H. S., and Wurster, W. H.: Shock Tube Study of Dissociation Relaxation in Oxygen. Jour. Chem. Phys. (Letters to the Editor), vol. 27, no. 5, Nov. 1957, pp. 1224–1226.
39. Camac, M., Camm, J., Keck, J., and Petty, C.: Relaxation Phenomena in Air Between 3000 and 8000° K. Res. Rep. 22 (Contract AF 04(645)–18), AVCO Res. Lab., Mar. 1958.
40. Gilles, A., and Vodar, B.: Variation With Temperature of the Transparency of Some Optical Materials in the Schumann Region. Jour. Optical Soc. of America (Letters to the Editor), vol. 42, no. 10, Oct. 1952, pp. 783–784.
41. Stockbarger, Donald C.: The Production of Large Single Crystals of Lithium Fluoride. Rev. Sci. Instr., vol. 7, no. 3, Mar. 1936, pp. 133–136.
42. Stockbarger, Donald C.: Artificial Fluorite. Jour. Optical Soc. of America, vol. 39, no. 9, Sept. 1949, pp. 731–740.
43. Bleakney, Walker, Weimer, D. K., and Fletcher, C. H.: The Shock Tube: A Facility for Investigations in Fluid Dynamics. Rev. Sci. Instr., vol. 20, no. 11, Nov. 1949, pp. 807–815.
44. Resler, E. L., Lin, Shao-Chi, and Kantrowitz, Arthur: The Production of High Temperature Gases in Shock Tubes. Jour. Appl. Phys., vol. 23, no. 12, Dec. 1952, pp. 1390–1399.
45. Hertzberg, A., and Smith, W. E.: A Method for Generating Strong Shock Waves. Jour. Appl. Phys. (Letters to the Editor), vol. 25, no. 1, Jan. 1954, pp. 130–131.
46. Glass, I. I., and Patterson, G. N.: A Theoretical and Experimental Study of Shock-Tube Flows. Jour. Aero. Sci., vol. 22, no. 2, Feb. 1955, pp. 73–100.
47. Russo, Anthony L., and Hertzberg, A.: Modifications of the Basic Shock Tube To Improve Its Performance. Rep. No. AD–1052–A–7 (AFOSR TN 58–716, AD 162 251), Cornell Aero. Lab., Inc., Aug. 1958.
48. Duff, Russel E.: Shock-Tube Performance at Low Initial Pressure. The Physics of Fluids, vol. 2, no. 2, Mar.-Apr. 1959, pp. 207–216.
49. Chubb, T. A.: Transmission of Barium Fluoride Crystal in the Ultraviolet. Jour. Optical Soc. of America (Letters to the Editor), vol. 46, no. 5, May 1956, pp. 362–363.
50. Purcell, J. D.: Reflectance Measurements From 1140A to 1190A by a Simple Open Air Method. Jour. Optical Soc. of America, vol. 43, no. 12, Dec. 1953, pp. 1166–1169.
51. Hass, G., Hunter, W. R., and Tousey, R.: Reflectance of Evaporated Aluminum in the Vacuum Ultraviolet. Jour. Optical Soc. of America, vol. 46, no. 12, Dec. 1956, pp. 1009–1012.
52. Johnson, Peter D.: Vacuum Ultraviolet Monochromator. Jour. Optical Soc. of America (Letters to the Editor), vol. 42, no. 4, Apr. 1952, pp. 278–279.
53. Hartman, P. L., and Nelson, J. R.: Hydrogen Lamp of Good Intensity and Reliability for the Vacuum Ultraviolet. Jour. Optical Soc. of America, vol. 47, no. 7, July 1957, pp. 646–648.
54. Wilkinson, P. G., and Tanaka, Yoshio: New Xenon-Light Source for the Vacuum Ultraviolet. Jour. Optical Soc. of America, vol. 45, no. 5, May 1955, pp. 344–349.
55. Wilkinson, P. G.: New Krypton Light Source for the Vacuum Ultraviolet. Jour. Optical Soc. of America, vol. 45, no. 12, Dec. 1955, pp. 1044–1046.
56. Lyman, Theodore: The Reversal of the Hydrogen Series in the Extreme Ultra-Violet. Science (Discussion), vol. LXIV, no. 1647, July 23, 1926, pp. 89–90.
57. Worley, R. Edwin: An Improved Source for the Lyman Continuum in the Vacuum Ultraviolet. Rev. Sci. Instr., vol. 13, no. 2, Feb. 1942, pp. 67–71.
58. Malmberg, J. H.: Millimicrosecond Duration Light Source. Rev. Sci. Instr., vol. 28, no. 12, Dec. 1957, pp. 1027–1029.

59. Weeks, Richard F.: A Simple Pulsed Ultraviolet Light Source. Tech. Note 15 (AFOSR–TN–58–615, ASTIA Doc. AD 162–143), Inst. Optics, Univ. of Rochester, Sept. 1958.

60. Brody, Seymour Steven: Instrument To Measure Fluorescence Lifetimes in the Millimicrosecond Region. Rev. Sci. Instr., vol. 28, no. 12, Dec. 1957, pp. 1021–1026.

61. Carpenter, R. O'B.: Radiation Sources for the Vacuum Ultraviolet. Final Tech. Rep., Contract No. AF 19(122)–432, Baird Assoc., Inc. (Cambridge, Mass.), Nov. 3, 1952.

62. Dieke, G. H., and Cunningham, S. P.: A New Type of Hydrogen Discharge Tube. Jour. Optical Soc. of America, vol. 42, no. 3, Mar. 1952, pp. 187–189.

63. Thurnau, Donald H.: Quantum Efficiency Measurements on Several Phosphors Under Excitation in the Extreme Ultraviolet. Jour. Optical Soc. of America, vol. 46, no. 5, May 1956, pp. 346–349.

64. Martinson, O., Isaacs, P., Brown, H., and Ruderman, I. W.: Rise Times of Voltage Pulses From Photo-Multipliers. Phys. Rev., vol. 79, no. 1, Second ser., July 1, 1950, p. 178.

65. Colden, Joseph A., and Myerson, Albert L.: Improved, Single Flash, Continuum Source for Use Below 2000 A. Jour. Optical Soc. of America, vol. 48, no. 8, Aug. 1958, pp. 548–550.

66. Schexnayder, Charles J., Jr.: On the Performance of a Double-Diaphragm Shock Tube Using the Reflected-Shock Method and a Light-Gas Buffer. Jour. Aero Space Sci. (Readers' Forum), vol. 25, no. 8, Aug. 1958, pp. 527–528.

67. Jones, Jim J.: Experimental Investigation of Attenuation of Strong Shock Waves in a Shock Tube With Hydrogen and Helium as Driver Gases. NACA TN 4072, 1957.

68. Lundquist, George A.: The NOL 8 x 8 Inch Shock Tube: Instrumentation and Operation. NAVORD Rep. 2449 (Aeroballistic Res. Rep. 100), U.S. Naval Ord. Lab. (White Oak, Md.), June 11, 1952.

69. Parkinson, W. W., Jr., and Williams, Ferd E.: A Vacuum Ultraviolet Monochromator for Absorption and Photoconductivity Measurements on Luminescent Solids. Jour. Optical Soc. of America, vol. 39, no. 8, Aug. 1949, pp. 705–708.

70. Anon.: Du Mont Multiplier Photo Tubes. Second Ed., Allen B. Du Mont Labs., Inc. (Clifton, N. J.), c.1959.

71. Byron, Stanley R.: Measurement of the Rate of Dissociation of Oxygen. Jour. Chem. Phys., vol. 30, no. 6, June 1959, pp. 1380–1392.

72. Griffith, Wayland C., and Kenny, Anne: States of Partial Equilibrium Behind Shock Waves in O_2, N_2, CO, CO_2 and N_2O. Tech. Rep. II 23 (Contract N6ori–105), Dept. Phys., Princeton Univ., Mar. 1957.

73. Hilsenrath, Joseph, Beckett, Charles W., et al.: Tables of Thermal Properties of Gases. NBS Cir. 564, U.S. Dept. Commerce, 1955, p. 430.

74. Fickett, W., and Cowan, R. D.: Values of Thermodynamic Functions to 12000° K for Several Substances. Jour. Chem. Phys., vol. 23, no. 7, July 1955, pp. 1349–1350.

75. Staff of the Computation Laboratory: The Annals of the Computation Laboratory of Harvard University. Vol. II Tables of the Modified Hankel Functions of Order One-Third and of Their Derivatives. Harvard Univ. Press, 1945.

TABLE I.—THE ABSORPTION COEFFICIENT OF OXYGEN AT SELECTED WAVE LENGTHS AND TEMPERATURES

T, °K	Absorption coefficient $\hat{k}$ at –										
	λ = 1,300A	λ = 1,350A	λ = 1,400A	λ = 1,450A	λ = 1,470A	λ = 1,500A	λ = 1,550A	λ = 1,600A	λ = 1,660A	λ = 1,700A	λ = 1,750A
Best estimate; all states excited											
300	0	0.425	0.985	0.995	0.940	0.822	0.583	0.335	0.135	0.060	0.018
1,000	-----	.424	.937	.903	.847	.744	.549	.351	.180	.104	.053
2,000	-----	.400	.808	.715	.670	.590	.471	.353	.229	.170	.112
3,000	-----	.359	.674	.580	.543	.495	.407	.330	.242	.198	.143
4,000	.207	.304	.559	.483	.457	.422	.360	.303	.237	.197	.153
5,000	.185	.251	.466	.404	.385	.358	.316	.272	.222	.189	.153
6,000	.158	.216	.394	.343	.332	.307	.275	.240	.200	.175	.148
7,000	.130	.189	.335	.296	.288	.270	.245	.217	.180	.163	.138
8,000	.105	.168	.291	.260	.253	.243	.221	.197	.170	.153	.132
9,000	.081	.153	.255	.228	.224	.218	.200	.182	.158	.144	.125
10,000	.058	.140	.227	.202	.200	.197	.182	.169	.147	.135	.119
Corrected; all states excited											
300	0	0.425	0.985	0.995	0.940	0.822	0.583	0.335	0.135	0.060	0.018
1,000	0	.420	.937	.903	.847	.744	.549	.351	.180	.104	.053
2,000	0	.350	.808	.715	.670	.590	.471	.353	.229	.170	.112
3,000	0	.278	.674	.580	.543	.495	.407	.330	.242	.198	.143
4,000	0	.228	.559	.483	.457	.422	.360	.303	.237	.197	.153
5,000	0	.191	.466	.404	.385	.358	.316	.272	.222	.189	.153
6,000	0	.159	.394	.343	.332	.307	.275	.240	.200	.175	.148
7,000	0	.134	.335	.296	.288	.270	.245	.217	.180	.163	.138
8,000	0	.115	.291	.260	.253	.243	.221	.197	.170	.153	.132
9,000	0	.103	.255	.228	.224	.218	.200	.182	.158	.144	.125
10,000	0	.091	.227	.202	.200	.197	.182	.169	.147	.135	.119
Uncorrected; all states excited											
300	0.216	0.545	0.862	1.000	0.970	0.870	0.625	0.370	0.158	0.075	0.028
1,000	.250	.557	.824	.903	.870	.781	.588	.387	.205	.124	.066
2,000	.314	.550	.706	.715	.681	.621	.508	.387	.259	.200	.138
3,000	.335	.510	.599	.583	.556	.517	.439	.362	.274	.224	.173
4,000	.338	.459	.512	.492	.471	.436	.383	.328	.263	.224	.185
5,000	.320	.411	.443	.420	.403	.377	.336	.294	.244	.214	.182
6,000	.300	.367	.385	.364	.350	.329	.295	.262	.224	.200	.173
7,000	.268	.326	.339	.317	.310	.289	.260	.236	.202	.183	.162
8,000	.253	.295	.303	.285	.276	.260	.233	.216	.188	.169	.155
9,000	.230	.267	.272	.257	.248	.235	.212	.195	.173	.157	.145
10,000	.208	.245	.246	.232	.225	.214	.193	.177	.160	.146	.135

TABLE I. THE ABSORPTION COEFFICIENT OF OXYGEN AT SELECTED WAVE LENGTHS AND TEMPERATURES Concluded

T, °K	Absorption coefficient $\hat{k}$ at -										
	λ=1,300A	λ=1,350A	λ=1,400A	λ=1,450A	λ=1,470A	λ=1,500A	λ=1,550A	λ=1,600A	λ=1,660A	λ=1,700A	λ=1,750A
Best estimate; $X(^3\Sigma_g^-)$ state only excited											
300	0	0.425	0.985	0.995	0.940	0.822	0.583	0.335	0.135	0.060	0.018
1,000	-----	.424	.937	.903	.847	.744	.549	.351	.180	.104	.053
2,000	-----	.404	.808	.715	.670	.590	.471	.353	.229	.170	.112
3,000	-----	.370	.690	.596	.558	.502	.417	.337	.247	.203	.144
4,000	.218	.328	.582	.504	.479	.439	.375	.315	.246	.203	.160
5,000	.210	.286	.503	.440	.423	.393	.343	.292	.239	.203	.165
6,000	.191	.257	.442	.389	.375	.354	.316	.273	.228	.198	.165
7,000	.169	.234	.393	.350	.340	.323	.290	.255	.215	.190	.163
8,000	.150	.216	.354	.315	.310	.294	.268	.238	.205	.181	.158
9,000	.134	.202	.321	.287	.285	.272	.249	.224	.195	.175	.155
10,000	.118	.187	.292	.262	.262	.258	.232	.210	.188	.170	.151
Corrected; $X(^3\Sigma_g^-)$ state only excited											
300	0	0.425	0.985	0.995	0.940	0.822	0.583	0.335	0.135	0.060	0.018
1,000	0	.420	.937	.903	.847	.744	.549	.351	.180	.104	.053
2,000	0	.350	.808	.715	.670	.590	.471	.353	.229	.170	.112
3,000	0	.287	.690	.596	.558	.502	.417	.337	.247	.203	.144
4,000	0	.243	.582	.504	.479	.439	.375	.315	.246	.203	.160
5,000	0	.208	.503	.440	.423	.393	.343	.292	.239	.203	.165
6,000	0	.179	.442	.389	.375	.354	.316	.273	.228	.198	.165
7,000	0	.157	.393	.350	.340	.323	.290	.255	.215	.190	.163
8,000	0	.140	.354	.315	.310	.294	.268	.238	.205	.181	.158
9,000	0	.126	.321	.287	.285	.272	.249	.224	.195	.175	.155
10,000	0	.114	.292	.262	.262	.258	.232	.210	.188	.170	.151
Uncorrected; $X(^3\Sigma_g^-)$ state only excited											
300	0.216	0.545	0.862	1.000	0.970	0.870	0.625	0.370	0.158	0.075	0.028
1,000	.250	.557	.824	.903	.870	.781	.588	.387	.205	.124	.066
2,000	.298	.550	.706	.715	.681	.621	.508	.387	.259	.200	.138
3,000	.339	.521	.608	.592	.567	.524	.447	.369	.279	.230	.176
4,000	.350	.483	.534	.514	.491	.457	.400	.342	.276	.235	.193
5,000	.343	.445	.478	.455	.437	.409	.363	.317	.267	.232	.196
6,000	.332	.411	.433	.410	.396	.372	.332	.295	.253	.226	.196
7,000	.316	.383	.397	.373	.359	.341	.308	.277	.239	.217	.193
8,000	.300	.358	.366	.343	.331	.314	.285	.260	.226	.206	.185
9,000	.286	.335	.340	.319	.309	.290	.266	.243	.215	.197	.180
10,000	.273	.315	.314	.300	.287	.273	.248	.227	.204	.190	.173

U.S. GOVERNMENT PRINTING OFFICE: 1962